



Aerosol characterization in a Central-West site of Brazil: influence of farming activities and toxicity

Yendry Jomolca Parra¹ · Guilherme Martins Pereira^{1,2} · Danilo Custódio^{1,3} · Sérgio Batista de Figueiredo⁴ · Célia Alves³ · Pérola de Castro Vasconcellos¹

Received: 26 May 2023 / Accepted: 2 November 2023 / Published online: 13 December 2023
© The Author(s), under exclusive licence to Springer Nature B.V. 2023

Abstract

The Central-West region of Brazil presents three important and large ecosystems: the Amazon, the *Cerrado*, and the *Pantanal* biomes. Different anthropogenic activities (e.g., biomass burning and land use) affect this area, emitting particulate matter (PM) that can be transported to urban sites, adding to the local vehicular sources. Sampling of atmospheric particulate material with a size less than and equal to 10 μm (PM_{10}) was carried out in the medium-sized city of Cuiabá (Brazil), between 2008 and 2014. The maximum concentrations of PM_{10} were found in the dry season, surpassing the recommended levels by the World Health Organization. A slight seasonal variation was found between the concentrations of organic carbon, elemental carbon, elements, and water-soluble ions (WSI), with higher levels in the dry season, enhanced by biomass burning and dust resuspension. Polycyclic aromatic hydrocarbons, their nitrated and oxygenated derivatives (nitro and oxy-PAHs), and some *n*-alkanes showed similar behaviors in the dry and rainy seasons, with higher abundance of carcinogenic PAHs compared to the rest of the polyaromatics. Total incremental lifetime cancer risks due to exposure to PAHs were found to exceed the safety level. Based on the application of diagnostic ratios and the positive matrix factorization receptor model, biomass burning, soil and road dust resuspension, vehicular exhaust, and mining activities were pointed out as emission sources. These results allow us to better understand the aerosol sources that contribute to the worsening of air quality in a growing urban area.

Keywords Biomass burning · Atmospheric particulate matter · Organic pollutants · Water-soluble ions · Air mass trajectories

Introduction

Exposure to airborne particles and the different chemical species associated with them can cause harmful effects on human health, fauna, and flora (de Oliveira Alves et al. 2020; Fajersztajn et al. 2017; Gurjar et al. 2010). These particles can contribute

to radiative forcing, as they can absorb or scatter light (Myhre 2013). Approximately 92% of the world's population lives in regions where air pollution levels exceed WHO guidelines. On the South American continent, especially in growing Brazilian cities, air pollution is a great challenge. In Brazil, air pollution is responsible for more than 51,000 deaths per year. It may lead to premature deaths, lung, and vascular diseases, as well as to the development of different types of cancer and other diseases (PAHO 2018; Sant'anna et al. 2021). Another aspect directly affected by air pollution is the Brazilian economy, registering losses in agricultural productivity (Roy and Braathen 2017).

Crop and forest fires are the main sources of air pollutant emissions in the regions of central Brazil and the Amazon. Biomass burning associated with deforestation and pasture management releases greenhouse gases and large amounts of particulate matter (Artaxo et al. 2013; Liu et al. 2020), increasing in the dry period, from July to October (Artaxo et al. 2013; de Oliveira Alves et al. 2015; de Oliveira Galvão et al. 2018). The central area of Brazil (including parts of the

✉ Yendry Jomolca Parra
yjomolcaparra@gmail.com

¹ Departamento de Química Fundamental, Instituto de Química, Universidade de São Paulo, São Paulo 05508-000, Brazil

² Departamento de Ciências Atmosféricas, Instituto de Astronomia, Geofísica e Ciências Atmosféricas, Universidade de São Paulo, São Paulo 05508-090, Brazil

³ Department of Environment and Planning, Centre for Environmental and Marine Studies (CESAM), University of Aveiro, 3810-193 Aveiro, Portugal

⁴ Secretaria do Estado de Meio Ambiente de Mato Grosso (SEMA-MT), Mato Grosso 78000, Brazil

Legal Amazon) is not only home to savannas and tropical rainforests (Sisenando et al. 2011) but also hosts one of the greatest soy productions in the world (FAO 2022). In the last decades, mineral exploration, industry, agriculture, and livestock have grown throughout this area and have caused an increase in fires used as a pretext for indiscriminate slaughter and burning for the development of agricultural or pastoral lands (Piromal et al. 2008). Urban areas have grown in this Brazilian region, where the studied city of Cuiabá is located. These growing urban areas in Brazil and other Latin American countries need further studies on air quality, given that most of the monitoring is concentrated in metropolises such as São Paulo and Rio de Janeiro (Squizzato et al. 2021).

Many health and environmental effects can be associated with the composition of particulate matter (PM). $PM_{2.5}$ and PM_{10} (PM with an aerodynamic diameter smaller than 2.5 and 10 μm , respectively) constituents include organic carbon (OC) and elemental carbon (EC) (Gurjar et al. 2010), potentially toxic metals and metalloids, such as As and Pb, and water-soluble secondary ions, as ammonium, sulfate, and nitrate (Pereira et al. 2017; Pereira et al. 2023a). EC is an important solar radiation absorber and is emitted mainly by the incomplete combustion of fossil fuels, including vehicular exhaust (especially heavy-duty vehicles) and biomass burning (Cao et al. 2021; de Oliveira Alves et al. 2015; Pio et al. 2011). Another important component of atmospheric aerosols is OC, representing up to 70% of the fine aerosols' total mass. It is related to diverse organic species such as aliphatic compounds and polycyclic aromatic hydrocarbons (PAHs), among others (Ding et al. 2009, 2019). PAHs represent a much studied class of contaminants since some of these species present carcinogenic and mutagenic properties (de Oliveira Galvão et al. 2018; Vasconcellos et al. 2011).

This study aimed at evaluating seasonal variations of PM_{10} concentration during the years 2008–2014, assessing the chemical composition of PM_{10} , estimating cancer risks resulting from exposure to elements and PAHs, and apportioning the contribution of different emission sources using diagnostic ratios, correlations between species, and the PMF receptor model.

Material and methods

Study area and fire maps

The studied site (coordinates: 15° 34' 11" S, 56° 04' 27" W) shown in Figure S1 corresponds to the parking lot of the Secretary of State for the Environment (SEMA) in Cuiabá (Capital of Mato Grosso State, Brazil). The sampling site is surrounded by several main avenues and large parking lots (light and heavy-duty vehicles). The industrial district is about 13 km away. The vegetation around is diverse, with

a predominance of the *Cerrado*, similar to savanna biome (Valente et al. 1982). The site is characterized by a tropical super-humid monsoon, with a high average annual temperature above 24 °C and high rainfall (2000 mm per year), concentrated in the wet season (Cavalcanti et al. 2009). The fires in the state occur mainly in the dry season, from May to October. Data from heat sources (fires) are detected by the National Oceanic and Atmospheric Administration (NOAA) satellite and are available from the National Institute for Space Research (INPE).

PM_{10} sampling

One hundred forty-six PM_{10} samples (Table S1) were collected between 2008 and 2014 with high-volume samplers (107 samples in the dry season and 39 samples in the wet season, one sample collected every three days, at a flow of 1.13 $\text{m}^3 \text{min}^{-1}$). Quartz fiber filters (20 cm \times 25 cm, Millipore, US) were used to collect the samples, which were previously treated at 800 °C for 8 h to eliminate organic contamination. The quartz fiber filters were stabilized (50% humidity) and then weighed on an analytical balance. The mass concentrations of PM_{10} were obtained by gravimetry (weighing before and after sampling). Once weighed, they were packed in aluminum foil, labeled, and stored at 5 °C until analysis (Boonyatumanond et al. 2007; Caumo et al. 2018).

Chemical characterization

To determine the organic carbon (OC) and elemental carbon (EC) content, the thermo-optical methodology detailed in Custódio et al. (2014) and Pio et al. (2011) was followed. The calculation of the uncertainty of this method (less than 5%) was based on the triplicate analysis of the filters. The detection limits were 30 ng m^{-3} for OC and 3 ng m^{-3} for EC. Organic matter (OM) was estimated by multiplying the OC concentrations by a factor of 1.6 (Pio et al. 2008).

Eight water-soluble inorganic species (WSI) were determined (Na^+ , K^+ , Mg^{2+} , Ca^{2+} , NH_4^+ , Cl^- , NO_3^- , and SO_4^{2-}) using the procedure described by Custódio et al. (2016). The determination of these species was carried out using four 9 mm circles cut from the filters and subjected to extraction with 5 mL of Milli-Q ultrapure water under an ultrasonic bath for 15 min. Subsequently, the liquid extracts were filtered through a 0.45 μm pore PTFE filter to remove insoluble particles. The different cations and anions were determined using an ion chromatograph (DIONEX, ICS-2500/2000). The method presents detection limits ranging from 0.1 to 1 ng m^{-3} .

Elemental determination was performed by inductively coupled plasma mass spectrometry (ICP-MS).

Approximately $\frac{1}{8}$ of each filter was acid digested (5 mL HF, 2.5 mL HNO₃, and 2.5 mL HClO₄) by mechanical agitation (5 h, 115 rpm at room temperature). Prior to ICP-MS analysis, samples were filtered through PTFE syringe filters with a pore size of 0.45 μm (Amato et al. 2016; Querol et al. 2001).

Elements' hazard quotient (HQ), for Mn, Cu, Co, Ni, Cd, and Pb, were calculated with Eqs. (1), (2), and (3) and indicate the non-carcinogenic risk of a single contaminant. The hazard index (HI), calculated with Eq. 4, which represents the total number of non-carcinogenic risks of the different contaminants for the three forms of exposure (ingestion, inhalation, and dermal contact) was also estimated (Hu et al. 2012; Jadoon et al. 2020; Zhou et al. 2014). HI is a non-cancerous risk due to multiple pathways. If $\text{HI} > 1$, it indicates that the metal may represent a non-carcinogenic risk for the public. However, if $\text{HI} \leq 1$, it can be concluded that the risk is insignificant. RfD_o is the reference dose and RfC_i reference concentration for inhalation, which means the maximum dose required to avoid an adverse reaction when absorbed, per unit time and per unit weight (Men et al. 2018; Gao et al. 2013). GIABS is a gastrointestinal absorption factor. SLF is the cancer slope factor, UIR is the metal inhalation unit hazard. RfD_o , RfC_i , SLF, GIABS, and IUR were downloaded from the US EPA site and provided in Table S2 (EPA 2023).

$$\text{HQ}_{\text{Ingestion}} = \frac{\text{DIM}_{\text{Ingestion}}}{\text{RfD}_o} \quad (1)$$

$$\text{HQ}_{\text{Inhalation}} = \frac{\text{EC}_{\text{Inhalation}}}{\text{RfC}_i \times 1000 \mu\text{g m}^{-3}} \quad (2)$$

$$\text{HQ}_{\text{Dermal}} = \frac{\text{DAD}_{\text{Dermal}}}{\text{RfD}_o \times \text{GIABS}} \quad (3)$$

$$\text{HI} = \sum \text{HQ}_{(\text{Ingestion/Inhalation/Dermal})} \quad (4)$$

Daily metal intake (DIM) was calculated with Eq. (5), dermal adsorption dose (DAD), with Eq. (6), and the exposure concentration (EC), with Eq. (7), in order to assess exposure through ingestion, dermal contact, and inhalation ($\text{mg kg}^{-1} \text{day}^{-1}$) (Hu et al. 2012; Jadoon et al. 2018). Cs is the element concentration (mg kg^{-1}) in PM₁₀ (EPA 2023), IR_{ing} is the ingestion rate, EF is the exposure frequency, ED is the exposure duration, BW is the average body weight, AT is the average time of illness development, CF is the conversion factor, IR_{inh} is the inhalation rate, PEF is the particle emission factor, SA is the surface area of the skin exposed to the airborne particles, AF is the dermal adherence factor for the air particulates, and ABS is dermal absorption factor. The values and units of all these parameters are given in Table S3.

$$\text{DIM}_{\text{Ingestion}} = \frac{(C_{\text{UCL}} \times \text{IR}_{\text{ing}} \times \text{EF} \times \text{ED})}{\text{BW} \times \text{AT} \times \text{CF}} \quad (5)$$

$$\text{EC}_{\text{Inhalation}} = \frac{(C_{\text{UCL}} \times \text{IR}_{\text{inh}} \times \text{EF} \times \text{ED})}{\text{BW} \times \text{AT} \times \text{PEF}} \quad (6)$$

$$\text{DAD}_{\text{Dermal}} = \frac{(C_{\text{UCL}} \times \text{SA} \times \text{AF} \times \text{ABS} \times \text{EF} \times \text{ED})}{\text{BW} \times \text{AT} \times \text{CF}} \quad (7)$$

The incremental lifetime cancer risk (ILCR) was calculated for Cd, Cr, Ni, and Pb with Eqs. 8, 9, and 10. In the current study, it is assumed that all metal risks were additive; therefore, it is possible to calculate the cumulative risk of cancer (Eq. 11) (Table S3). The tolerable risk for regulatory purposes is in the range of 1×10^{-6} – 1×10^{-4} provided by Jadoon et al. (2018), Men et al. (2018), and Zhang et al. (2017).

$$\text{ILCR}_{\text{Ingestion}} = \text{DIM} \times \text{SLF} \quad (8)$$

$$\text{ILCR}_{\text{Dermal}} = \text{DAD} \times \left(\frac{\text{SLF}}{\text{GIABS}} \right) \quad (9)$$

$$\text{ILCR}_{\text{Inhalation}} = \text{IUR} \times \text{EC} \quad (10)$$

$$\text{ILCR}_{\text{Total}} = \sum \text{ILCR}_i \quad (11)$$

The organic material deposited on the filters was extracted by sonication with dichloromethane (80 mL) from circular portions (9 mm in diameter), with three cycles of 20 min. Then, the extract was concentrated to 1 mL in a rotary evaporator (Pereira et al. 2017). A glass column containing 3.2 g of silica gel and 1.8 g of alumina was used to separate the different classes of compounds in the organic extracts. Two fractions were collected, the first contained alkanes (40 mL of hexane), and the second, PAHs and derivatives (50 mL of hexane + 50 mL of methylene chloride); then, each fraction was evaporated until 1 mL. The extracts were dried using a low and constant flow of N₂ at room temperature (Caumo et al. 2018; Krůmal et al. 2013). PAHs, nitro-PAHs, and oxy-PAHs were quantified in a gas chromatograph coupled to a mass spectrometer (GC-MS) (Agilent Technology) equipped with a VF-5ms (30 m \times 0.25 mm \times 0.25 μm) column. The qualitative and quantitative analyses of PAHs and their derivatives were performed using the methodology detailed in de Oliveira Alves et al. (2015). *N*-alkane (C₁₆–C₄₀) concentrations were determined using a gas chromatograph with a flame ionization detector (GC-FID, Shimadzu, 2010) equipped with a SH-Rtx-5 column (30 m \times 0.32 mm \times 0.25 mm). Other details are described in Caumo et al. (2018).

Fifteen PAHs were quantified, including fluorene (Flu), phenanthrene (Phe), and anthracene (Ant) with 3 rings;

fluoranthene (Flt), pyrene (Pyr), benzo[a]anthracene (BaA), and chrysene (Chry) with 4 rings; benzo[b]fluoranthene (BbF), benzo[k]fluoranthene (BkF), benzo[e]pyrene (BeP), benzo[a]pyrene (BaP), and dibenzo[a,h]anthracene (DahA) with 5 rings; and indeno[1,2,3-cd]pyrene (InP) and benzo[ghi]perylene (BghiP) with 6 rings and coronene (Cor) with 7 rings. These PAHs can be classified according to their molecular weight: low (3-ring LMW-PAHs), medium (4-ring MMW-PAHs), and high (5, 6, and 7-ring HMW-PAHs). In addition, nine nitro-PAHs and four oxygenated PAHs were determined. They were 9-nitrophenanthrene (9-NPhe), 6-nitrochrysene (6-NChry), 1-nitropyrene (1-NPyr), 4-nitropyrene (4-NPyr), 3-nitrofluoranthene (3-NFlt), 2-nitrofluorene (2-NFlu), 7-nitrobenzo[a]anthracene (7-NBaA), 6-nitrobenzo[a]pyrene (6-NBaP), 5-nitroacenaphthene (5-NAce), 9,10-anthraquinone (9,10-AQ), 9-fluorenone (9-FO), 2-methylanthraquinone (2-MAQ), and benzo[a]anthra-7,12-quinone-(7,12-BAQ).

Analytical standards were used to construct calibration curves to determine analyte concentrations. The recovery percentages for the determined organic compounds varied between 65 and 102%, 69 and 112%, 98 and 114%, and 70 and 99 % for PAHs, nitro-PAHs, oxy-PAHs, and *n*-alkanes, respectively. The linearity of the curve was ($R^2 > 0.99$) for all compounds.

Benzo[a]pyrene equivalent carcinogenicity and mutagenicity

The benzo[a]pyrene (BaP) carcinogenic (BaP-TEQ) and mutagenic (BaP-MEQ) equivalents were calculated (de Oliveira Alves et al. 2015; Jung et al. 2010) by multiplying the PAH concentrations and the respective carcinogenicity (TEQ) or mutagenicity (MEQ) potential (Durant et al. 1996; Nisbet and LaGoy 1992; Jung et al. 2010), according to Eqs. 12 and 13. To estimate the BaP equivalent carcinogenicity for nitro-PAHs (BaP-TEQ_{nitro-PAH}), their concentrations were multiplied by the respective carcinogenic equivalent factors (TEQ) (de Oliveira Alves et al. 2015; Jung et al. 2010), as shown in Eq. 14.

$$\begin{aligned} \text{BaP-TEQ} = & ([\text{BaA}] \times 0.1) + ([\text{Chry}] \times 0.01) + ([\text{BbF}] \times 0.1) + ([\text{BkF}] \times 0.1) \\ & + ([\text{BaP}] \times 1) + ([\text{InP}] \times 0.1) + ([\text{DBA}] \times 5) + ([\text{BghiP}] \times 0.01) \end{aligned} \quad (12)$$

$$\begin{aligned} \text{BaP-MEQ} = & ([\text{BaA}] \times 0.082) + ([\text{Chry}] \times 0.017) + ([\text{BbF}] \times 0.25) \\ & + ([\text{BkF}] \times 0.11) + ([\text{BaP}] \times 1) + ([\text{InP}] \times 0.31) \\ & + ([\text{DBA}] \times 0.29) + ([\text{BghiP}] \times 0.19) \end{aligned} \quad (13)$$

$$\begin{aligned} \text{BaP-TEQ}_{\text{nitro-PAHs}} = & ([1\text{NPyr}] \times 0.1) \\ & + ([4\text{NPyr}] \times 0.1) \\ & + ([6\text{NChry}] \times 10) \end{aligned} \quad (14)$$

The incremental lifetime cancer risk (ILCR) was calculated to quantitatively estimate the risk of exposure through

inhalation, ingestion, and dermal uptake routes to environmental PAHs that are reported to be carcinogenic and mutagenic by applying the US EPA standard models (Eqs. 15, 16, and 17) (EPA 2011; 1993; Goudarzi et al. 2021; Yang et al. 2015). CS is the sum of BaP equivalent concentrations of individual PAHs, which were calculated based on the toxic equivalency factors (TEF) listed in Table 2 ($\mu\text{g kg}^{-1}$) (Nisbet and LaGoy 1992), CSF is the carcinogenic slope factor ($\text{mg kg}^{-1} \text{day}^{-1}$)⁻¹, BW is the body weight (kg), AT is the average life span (day), EF is the exposure frequency (day year^{-1}), ED is the exposure duration (years), $\text{IR}_{\text{Inhalation}}$ is the inhalation rate ($\text{m}^3 \text{day}^{-1}$), $\text{IR}_{\text{Ingestion}}$ is the soil intake rate (mg day^{-1}), SA is the dermal surface exposure (cm^2), AF is the dermal adherence factor ($\text{mg cm}^{-2} \text{h}^{-1}$), ABS is the dermal absorption fraction, and PEF is the particle emission factor ($\text{m}^3 \text{kg}^{-1}$). $\text{CSF}_{\text{Ingestion}}$, $\text{CSF}_{\text{Dermal}}$, and $\text{CSF}_{\text{Inhalation}}$ of BaP were taken as 7.3, 25, and 3.85 ($\text{mg kg}^{-1} \text{day}^{-1}$)⁻¹, respectively. These values were determined by the cancer-causing ability of BaP (Goudarzi et al. 2021; Minnesota Department of Health 2016; Peng et al. 2011). Cancer risks were estimated for three age groups: childhood (0–10 years), adolescence (11–18 years), and adulthood (19–70 years) (Table S3).

$$\text{ILCR}_{\text{Ingestion}} = \frac{\text{CS} \times \left(\text{CSF}_{\text{Ingestion}} \times \sqrt[3]{\frac{\text{BW}}{70}} \times \text{IR}_{\text{Ingestion}} \times \text{EF} \times \text{ED} \right)}{\text{BW} \times \text{AT} \times 10^6} \quad (15)$$

$$\text{ILCR}_{\text{Dermal}} = \frac{\text{CS} \times \left(\text{CSF}_{\text{Dermal}} \times \sqrt[3]{\frac{\text{BW}}{70}} \times \text{SA} \times \text{SAF} \times \text{ABS} \times \text{EF} \times \text{ED} \right)}{\text{BW} \times \text{AT} \times 10^6} \quad (16)$$

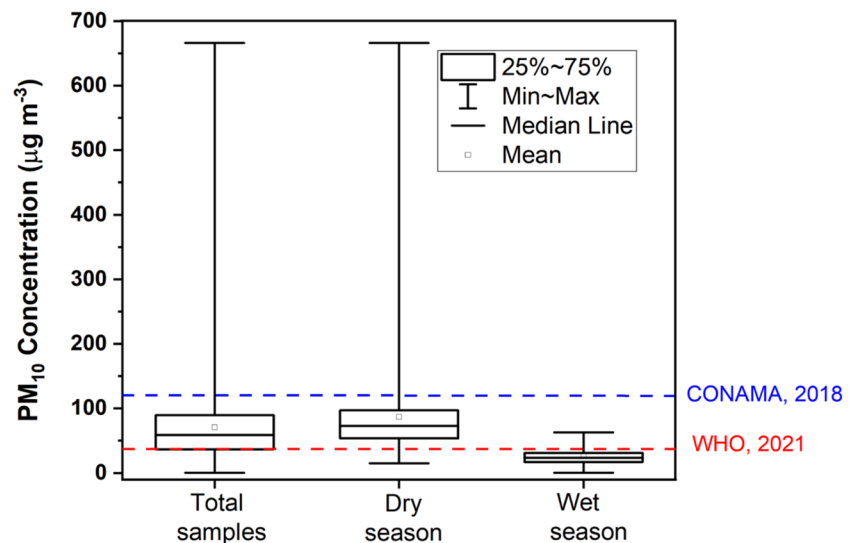
$$\text{ILCR}_{\text{Inhalation}} = \frac{\text{CS} \times \left(\text{CSF}_{\text{Inhalation}} \times \sqrt[3]{\frac{\text{BW}}{70}} \times \text{IR}_{\text{Inhalation}} \times \text{EF} \times \text{ED} \right)}{\text{BW} \times \text{AT} \times \text{PEF}} \quad (17)$$

Data treatment

Different diagnostic ratios between PAHs (Fla, Pyr, BaA, BbF, BkF, BaP, BghiP, and InP) are generally calculated to assign the main emission sources (Oliveira et al. 2011; Pereira et al. 2017). The carbon preference index (CPI) is also a diagnostic source ratio. When applied to *n*-alkanes, it is a proportionality ratio between homologs with an even carbon number and those with an odd carbon number (Eq. 18). It indicates whether the *n*-alkanes are of biogenic or anthropogenic origin. Likewise, C_{max} (the most abundant *n*-alkane in the homologous series) provides indication of biogenic or anthropogenic contributions (Caumo 2020; Simoneit 1984; Simoneit et al. 1990).

$$\text{CPI} = \frac{\sum \text{Concentration of odd carbon homologs}}{\sum \text{Concentration of even carbon homologs}} \quad (18)$$

Fig. 1 Concentrations of PM₁₀ collected during the whole period and in the dry and wet seasons (2008–2014)



The enrichment factor (EF) was used to identify the degree to which an element in the aerosol is enriched, by applying Eq. 19, where C_x/C_{Fe} is the ratio of elements in the PM₁₀ and in the crust reported in Lee (1999). The element Fe was used as reference crustal metal to calculate the EFs. EFs below 2 indicate minimal enrichment, between 2 and 5, moderate enrichment, between 5 and 20, significant enrichment, between 20 and 40 very high enrichment, and above 40, extremely high enrichment (Yang et al. 2016).

$$EF = \frac{(C_x/C_{Fe})_{PM10}}{(C_x/C_{Fe})_{Crust}} \quad (19)$$

In this study, the receptor model positive matrix factorization (PMF) was employed for source apportionment. The US EPA PMF v5 software was applied. The species that retain a significant signal were separated from those dominated by noise, following the signal-to-noise (S/N) criterion defined by Paatero and Hopke (2003). Species with $S/N < 0.2$ are generally defined as poor variables and removed from the analysis, and species with $0.2 < S/N < 2$ are typically defined as weak and weighted variables (increasing the uncertainty by a factor of 3). However, since the S/N is very sensitive to sporadic values above the noise level, the data percentage above the detection limit was used as an additional criterion. A set of 142 samples and 25 chemical species were used as input for the model.

The aerosol composition was examined by means of statistics and correlation analysis using the RStudio Free Software 2013 (Free Software Foundation's GNU General Public License) and Microsoft Excel 2013 (Microsoft Corp. USA). To compare (significant differences) the results obtained in the studied seasons, the Student's *T* test and the Mann-Whitney *U* test were used following the distribution. The distribution of the data was verified using the Shapiro-Wilk normality test. A significance level of 0.05 was used for the statistical tests.

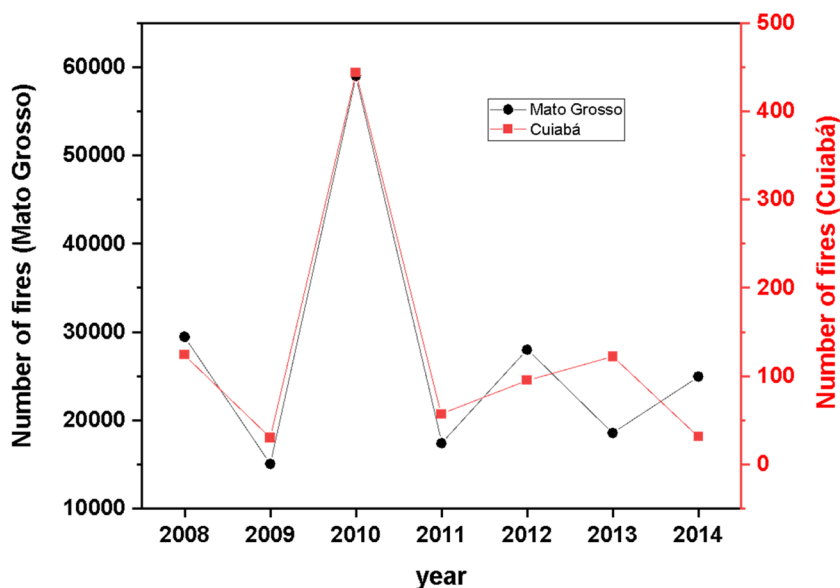
Results and discussion

PM₁₀ concentrations and air mass trajectories

The PM₁₀ concentrations in Cuiabá ranged between 1 and 666 $\mu\text{g m}^{-3}$, averaging $70 \pm 66 \mu\text{g m}^{-3}$ (Fig. 1). Comparing the average concentration obtained in this study with the values recommended by the new WHO guidelines (2021) (45 $\mu\text{g m}^{-3}$), the levels were higher in 69% of the samples. On the other hand, the limit of 120 $\mu\text{g m}^{-3}$ imposed by the Brazilian legislation (CONAMA 2018) was exceeded in 58% of the samples.

A mean value of 87 $\mu\text{g m}^{-3}$ was registered in the dry season, during which 87% of the samples presented values surpassing the WHO guideline. On the other hand, the mean obtained for the wet period was 27 $\mu\text{g m}^{-3}$, with 16% of the samples above the value recommended by the WHO (2021). The significant lower concentrations (Mann-Whitney; $p < 0.05$) found in the wet season may be due to the greater frequency of rains, which favor the wet deposition of the particulate material by washout and rainout processes, keep the soil wet and thus limit dust resuspension, and prevent fires because of the high moisture content of biomass. It has been reported that, in the rainy season, during which natural emissions predominate, the mass concentration of PM₁₀ in Amazonian regions ranges from 10 to 30 $\mu\text{g m}^{-3}$ (Artaxo et al. 2002; de Oliveira Alves et al. 2015; Santanna et al. 2016). Artaxo et al. (2013) obtained a PM₁₀ concentration of 57 $\mu\text{g m}^{-3}$, during a period of strong drought in 2010 in Rondônia. De Oliveira Alves et al. (2015) found a mean of 30 $\mu\text{g m}^{-3}$ in that site (dry season), between 2011 and 2012. In rural areas of Cuiabá (2004–2005), a concentration of 20 $\mu\text{g m}^{-3}$ was recorded for the same season. The value obtained in this work (87 $\mu\text{g m}^{-3}$) was higher than in those previous studies, but it is lower than that registered during

Fig. 2 Number of fires per year in Mato Grosso and Cuiabá (2008–2018) (INPE, 2022)



the dry season several years before ($100 \mu\text{g m}^{-3}$) by Maenhaut et al. (2002). Values also reached high levels (between 15 and $600 \mu\text{g m}^{-3}$) during the dry season in Alta Floresta, in the north of Mato Grosso state, and in Rondônia (Artaxo et al. 2002). According to Artaxo et al. (2002), the high concentrations of atmospheric particulate matter during the dry season result from the fires that occur in Alta Floresta and Rondônia, whose smoke spreads over an area of 5 million km^2 . Therefore, the effects of these emissions exceed the local scale and affect regions far from the sources on a regional and global scale.

Fig. 2 presents the fires reported between 2008 and 2014 in the state and its capital. The annual values exceeded 17,000 fires in Mato Grosso, representing approximately 14% of the total detected in the country during the studied period. Only 0.4% of the fires detected in Mato Grosso correspond to those registered in the Cuiabá municipality during the analyzed period (2008–2014).

The hybrid single-particle Lagrangian integrated trajectory (HYSPLIT) model was used to calculate the air mass backward trajectories (96 h) for each sampling period. Similar trajectories were grouped by cluster analysis (Draxler and Hess 1998). Fig. 3b, c shows that higher concentrations in the two seasons are observed when air masses originated in the southern and eastern sectors, suggesting the influence of pollution from these regions on aerosol mass loadings in Cuiabá. On August 13, 2014, the PM_{10} concentration was the highest ($666 \mu\text{g m}^{-3}$). This high value may be related to the huge number of fires registered in Mato Grosso state on that day (6200 fires), 3 to 4 times higher than on the other sampling days (Fig. 3a). Fig. 3d, e shows the average trajectories of the four clusters obtained for the two seasons. For both the dry and wet seasons, the highest PM_{10} loads were associated with air masses from the East and South,

accounting for 61 and 34% of the backward trajectories, respectively. However, in the wet season, air masses coming from the north were also significant.

Carbonaceous species, water-soluble inorganic ions, and elements

The mean concentrations, standard deviations, and ranges of OC, EC, OM, and TC are presented in Table 1. OC and EC concentrations ranged, respectively, from 0.1 to $24.7 \mu\text{g m}^{-3}$ and from 0.1 to $10.5 \mu\text{g m}^{-3}$, representing 9 and 4% of the total PM_{10} mass. During the dry period, the concentration of OC ($6.6 \mu\text{g m}^{-3}$) and EC ($2.9 \mu\text{g m}^{-3}$) were significantly higher than those obtained in the wet season (Mann-Whitney; $p < 0.05$), but the contribution of these species to PM_{10} was lower in this period, which may be attributed to a higher share of inorganic constituents in the dry season due to dust resuspension (Alves et al. 2018).

The OC/EC ratio in the present study was 2.6 ± 1.3 (2.6 in the dry season and 2.8 in the wet season, respectively). Values from 2 to 5 are found in urban background atmospheres and may indicate a significant contribution from secondary organic aerosol (Pio et al. 2011), while ratios near or less than one may reflect fresh traffic emissions (Alves et al. 2015; Pio et al. 2011; Pereira et al. 2023a). Authors such as Amato et al. (2016) and Pereira et al. (2017) have reported ratios between 1 and 2 for urban environments. Alves et al. (2015) and Gonçalves et al. (2016) observed that higher values in remote forested locations in the Amazon may be associated with biogenic organic aerosols and biomass burning. Therefore, the values now obtained can be attributed to contributions from secondary aerosols and biomass burning.

Higher EC and OM concentrations in the dry season compared to the wet season are probably a result of emissions

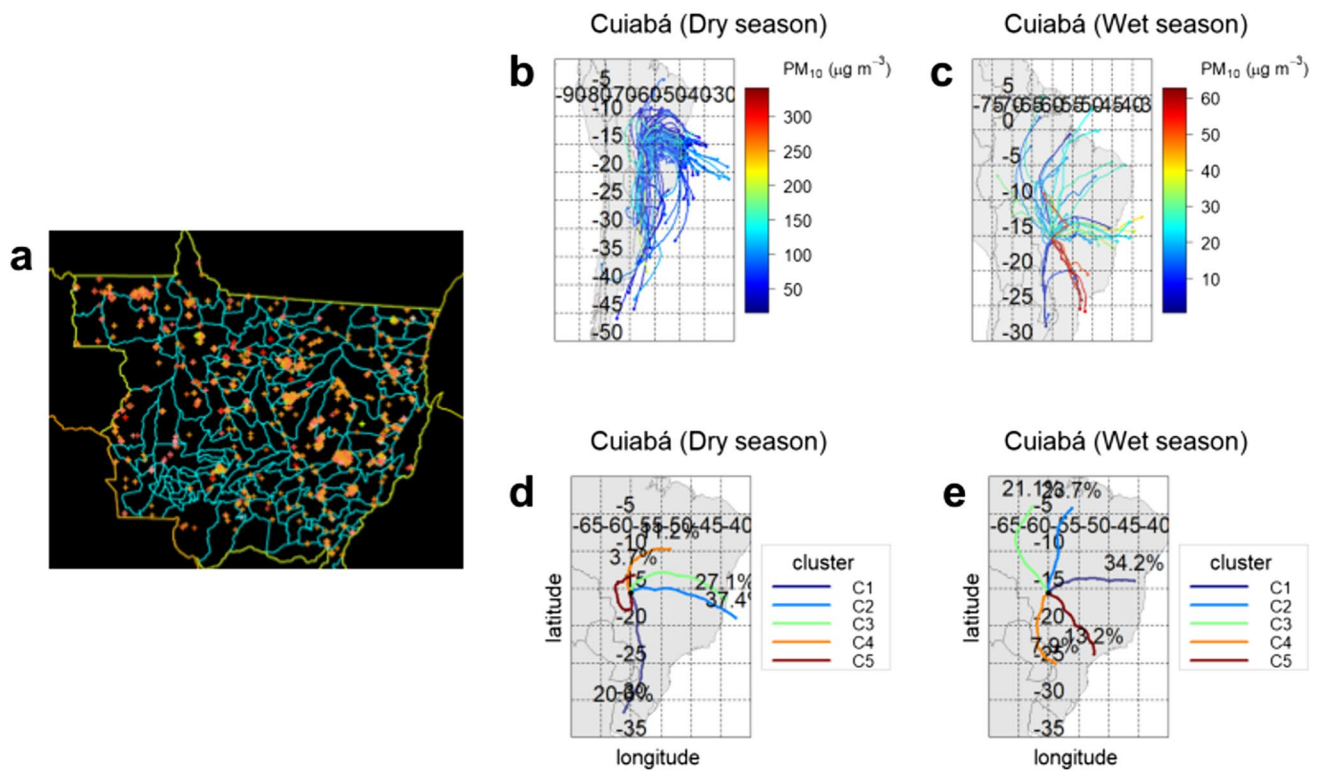


Fig. 3 Number of fires in Mato Grosso in the 12/08/2014–13/08/2014 period. (INPE, 2022) (a). Plots of backward trajectories as a function of PM_{10} concentrations ($\mu g\ m^{-3}$) (b, c). Cluster with trajectories of air masses (d, e)

Table 1 Carbonaceous species (OC and EC) and concentrations of total particulate organic matter (OM) observed in Cuiabá during the dry and wet seasons ($\mu g\ m^{-3}$)

		OC	EC	OC/EC	OM	TC
Total	Mean \pm SD	5.6 \pm 3.4	2.5 \pm 1.6	2.6 \pm 1.3	9.0 \pm 5.5	8.1 \pm 4.7
	Min-max	0.1–24.7	0.1–10.5	0.4–8.8	0.3–39.5	0.2–35.2
	Mean/ PM_{10} (%)	9	4	-	15	13
Dry season	Mean \pm SD	6.6 \pm 3.4	2.9 \pm 1.6	2.6 \pm 1.3	10.5 \pm 5.5	9.5 \pm 4.6
	Min-max	0.1–24.7	0.1–10.5	0.8–6.5	1.4–39.5	1.0–35.2
	Mean/ PM_{10} (%)	8	4	-	13	12
Wet season	Mean \pm SD	2.9 \pm 1.3	1.3 \pm 1.0	2.8 \pm 1.6	4.6 \pm 2.1	4.2 \pm 2.2
	Min-max	0.1–6.0	0.1–4.7	0.4–8.8	0.1–9.6	0.2–9.8
	Mean/ PM_{10} (%)	11	6	-	18	17

from fires and agricultural and forestry activities in the southern Amazon basin. On the other hand, the decrease in concentrations in the wet season can be attributed to unfavorable climatic conditions for dust resuspension and dispersion of particulate matter due to heavy rains (Custodio et al.

2019; Gonçalves et al. 2016; Santanna et al. 2016; Yamasoe et al. 2000).

The water-soluble inorganic species (WSI) determined in this study are shown in Table 2. Na^+ was the WSI with highest concentrations. It is well known that Na^+ and Cl^- are

Table 2 Total and seasonal concentrations of elements and water-soluble ions (ng m^{-3}) in PM_{10} for Cuiabá (LD-detection limit)

	Total		Dry season		Wet season	
	Mean \pm SD	Range	Mean \pm SD	Range	Mean \pm SD	Range
Na^+	2498 \pm 587	< LD–4839	2650 \pm 570	1586–4839	2049 \pm 350	< LD–2799
K^+	249 \pm 167	< LD–1535	283 \pm 180	27–1535	151 \pm 51	< LD–0.3
Mg^{2+}	100 \pm 55	< LD–302	118 \pm 52	30–302	51 \pm 20	< LD–95
Ca^{2+}	661 \pm 336	< LD–2184	777 \pm 301	178–2184	325 \pm 152	< LD–750
NH_4^+	21 \pm 22	< LD- 111	23 \pm 22	< LD–111	3 \pm 3	< LD–8
Cl^-	346 \pm 203	< LD–1520	409 \pm 193	84–1520	164 \pm 76	< LD–383
NO_3^-	1301 \pm 1018	< LD–7658	1559 \pm 1032	278–7658	535 \pm 379	< LD–1640
SO_4^{2-}	2322 \pm 607	< LD–3690	2461 \pm 592	1138–3960	1924 \pm 443	< LD–3041
Fe	8658 \pm 5810	2159–50265	9374 \pm 5888	2226–50265	3961 \pm 1529	2159–7031
Ga	11 \pm 7	7–24	12 \pm 3	8–24	10 \pm 1	7–12
Li	14 \pm 11	2–47	14 \pm 12	2–47	10 \pm 6	7–27
Be	0.5 \pm 0.2	0.1–1.3	0.5 \pm 0.2	0.1–1.3	0.4 \pm 0.1	0.3–0.6
V	11 \pm 10	2–105	12 \pm 11	2–105	5 \pm 2	2–9
Mn	63 \pm 31	12–163	68 \pm 31	13–163	36 \pm 12	24–66
Co	0.8 \pm 0.6	0.1–2.7	0.8 \pm 0.6	0.1–2.7	0.3 \pm 0.2	0.1–1.0
Ni	4 \pm 3	1–14	5 \pm 3	6–14	3 \pm 1	2–4
Cu	560 \pm 808	59–5157	572 \pm 842	59–5157	482 \pm 520	145–2015
As	4 \pm 2	1–11	5 \pm 2	1–11	3 \pm 1	2–4
Rb	52 \pm 46	7–186	54 \pm 48	7–186	37 \pm 27	25–109
Sr	278 \pm 165	42–762	284 \pm 173	42–762	234 \pm 89	187–485
Cd	4.0 \pm 6.5	0.2–22.5	4.3 \pm 6.7	0.2–22.5	2.0 \pm 4.0	0.4–12.8
Cs	1.4 \pm 1.9	0.1–7.2	1.5 \pm 2.0	0.1–7.2	0.8 \pm 1.2	0.2–3.9
Tl	0.3 \pm 0.2	0.1–0.9	0.2 \pm 0.2	0.1–0.9	0.2 \pm 0.1	0.2–0.5
Pb	40 \pm 39	6–224	42 \pm 41	6–224	26 \pm 21	14–82

the main sea spray components (Custódio et al. 2016), but both ions can also be incorporated into particulate matter through biomass burning and dust resuspension (Seinfeld and Pandis 2006). Cl^-/Na^+ ratios were below 0.2 in both seasons, rather lower than the 1.8 ratio found in sea salt (Fu et al. 2004; Souza et al. 2014), corroborating to other sources of sodium and/or the depletion of Cl^- (Pereira et al. 2017). The other water-soluble species that presented high concentrations were K^+ and Ca^{2+} , being slightly higher during the dry season. K^+ is found in biomass burning emissions (de Oliveira Alves et al. 2015; Vasconcellos et al. 2007) and soil resuspension (Amato et al. 2016; Pereira et al. 2017). On the other hand, Ca^{2+} is associated with soil resuspension (Castanho and Artaxo 2001; Othman et al. 2021).

The relatively high concentrations of SO_4^{2-} and NO_3^- in the two seasons may be related to a contribution of secondary formation from anthropogenic-emitted gaseous precursors (industrial activities and vehicle emissions) (Pereira et al. 2017; Vasconcellos et al. 2011) (Table 3). Furthermore, higher year-round temperatures may reduce the formation and relative contribution of particulate nitrate in the studied site (Ianniello et al. 2011). The low molar concentrations of NH_4^+ during the studied period (1.2 nmol m^{-3}) may indicate that less than 2 % of H_2SO_4 could be

neutralized by ammonia. When the molar ratio $[\text{NH}_4^+]/[\text{SO}_4^{2-}]$ is higher than 2, excess NH_4^+ may indicate that HNO_3 may be also neutralized by ammonia (Sharma et al. 2016). Due to low ammonium concentrations, the neutralization of these acids could be carried out mainly by aerosols of carbonated minerals coming from the soil, especially in the dry season. The ammonium availability index (J) is calculated as follows:

$$J = \frac{[\text{NH}_4^+]}{2 \times ([\text{SO}_4^{2-}] + [\text{NO}_3^-])} \quad (20)$$

in percent related to the amount of ammonia available to neutralize acids. Considering ammonia as the only basic component of PM capable of neutralizing these acids, the J index can be used to estimate the acidity of the aerosol (Singh et al. 2021). The very low J index in the present study (below 2%) may indicate that the aerosol is considerably acidic throughout the campaign.

The WSI presented a larger contribution to the mass of PM_{10} in the dry season (22%) compared to the wet season (11%), which may be associated with the greater number of fires and enhanced dust resuspension in the most arid period (Artaxo et al. 2002; Martin et al. 2010). Na^+ , SO_4^{2-} ,

Table 3 Total and seasonal element diagnostic ratios for Cuiabá

Ratio	Total	Dry season	Wet season
Fe/Cu	32	34	15
Fe/Ca ²⁺	12	13	9
EC/Cu	11	11	6

NO₃⁻, Ca²⁺, and K⁺ showed significantly higher concentrations (Mann-Whitney; $p < 0.05$) during the dry season and together are often associated with crustal and soil resuspension sources (Pereira et al. 2017), apart from secondary formation for SO₄²⁻ and NO₃⁻. The other species presented less difference when compared to the wet period.

Overall, the most abundant elements were Fe > Cu > Sr > Mn > Rb > Pb. This profile is similar to that observed in Latin American urban sites such as São Paulo, Lima (Perú), and Medellín (Colombia) in the last decades (La Colla et al. 2021; de Oliveira Alves et al. 2020; Pereira et al. 2019; Pereira et al. 2017). The predominance of elements such as Fe and Cu have been associated with emissions from vehicles powered by ethanol and gasohol, widely used in Brazil (Brito et al. 2013). These elements have also been associated with non-exhaust sources (brake abrasion and road dust resuspension) (Thorpe and Harrison 2008). Pb emissions were recently linked to the Brazilian HDV fleet (Pereira et al. 2023a). Fe and Cu have been related to engine corrosion that increases with the use of ethanol fuel in Brazilian LDVs, while Cu is also present in ethanol (Ferreira da Silva et al. 2010; Pereira and Pasa 2005). Another abundant element, strontium has been associated with road dust in the coarse mode (Behera et al. 2015; Pereira et al. 2019). rubidium may be associated with soil and biomass burning emissions (Saide et al. 2020; Massimi et al. 2020).

Enrichment factors are displayed in Fig. 4. Overall, Be, V, Mn, Co, and Ni presented minimal enrichments. Some of these species, such as V and Ni, are often attributed to anthropogenic sources (e.g., fuel combustion), but showed low EFs here, which may be due to the regional characteristics of the soil. Mn is abundant in the crust (Lee 1999) and is therefore often associated with dust resuspension. However, it has also been related to vehicular sources (Pant and Harrison 2013). Pb, Cu, and As presented significant to very high enrichments. Copper has been described as an element of LDV emissions in Brazil (Brito et al. 2013), while As has multiple sources (Hedberg et al. 2005). Arsenic-rich particles have also been found in road dust affected by agricultural activities, which can release this element by livestock dips, pesticide application, organic manure, and fertilizers (Candeias et al. 2020; Punshon et al. 2017). Cadmium was extremely enriched and often originated from industrial sources (e.g., metal smelting, electroplating, and mining) (Zhong et al. 2020). The study of Csavina et al. (2011) associated the presence of toxic elements such as As, Cd, and Pb, to mining activities. In the dry season, overall, lower EFs were observed, suggesting a higher contribution of soil resuspension.

The diagnostic ratios between the elements are presented in Table 3. The average Fe/Cu ratio was 31, higher than that observed in a tunnel study in São Paulo in 2018 (4 and 9 for the Jânio Quadros and Rodoanel tunnels) (Pereira et al. 2023a), suggesting a greater influence of soil resuspension for iron. The observed values are also higher than those attributed to brake wear debris in dynamometer studies from two decades ago (Fe/Cu = 14) (Sanders et al. 2003) and in an urban road tunnel in Portugal (Fe/Cu = 21) (Pio et al. 2013). The Fe/Ca ratio (considering Ca²⁺) was, on average, 12. A Fe/Ca value of 20 was documented for emissions from

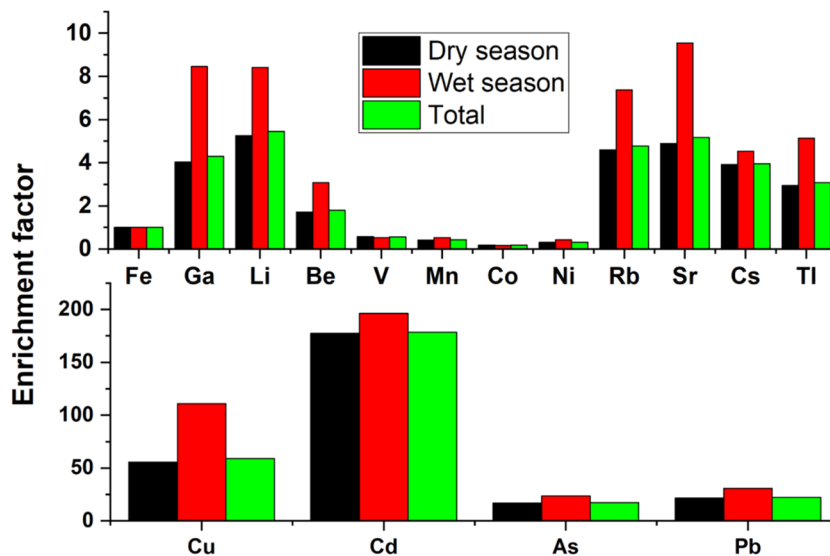
Fig. 4 Total and seasonal element enrichment factors for Cuiabá

Table 4 Non-cancerous hazard or risk index (HI) for each metal in Cuiabá (dry and wet seasons)

	Group	Mn HI	Co	Ni	Cu	Cd	Pb
Total	Children	2.9×10^{-4}	2.5×10^{-7}	1.6×10^{-7}	1.3×10^{-6}	4.3×10^{-6}	8.0×10^{-6}
Dry season		3.6×10^{-4}	3.2×10^{-7}	2.0×10^{-7}	1.6×10^{-6}	5.5×10^{-6}	1.0×10^{-4}
Wet season		8.3×10^{-5}	5.8×10^{-8}	5.3×10^{-8}	5.6×10^{-7}	1.1×10^{-6}	2.5×10^{-5}
Total	Adolesc.	2.4×10^{-4}	1.3×10^{-7}	1.3×10^{-7}	7.1×10^{-7}	3.5×10^{-6}	3.4×10^{-5}
Dry season		3.1×10^{-4}	1.7×10^{-7}	1.6×10^{-7}	8.6×10^{-7}	4.5×10^{-6}	4.3×10^{-5}
Wet season		7.0×10^{-5}	3.1×10^{-8}	4.3×10^{-8}	3.0×10^{-7}	8.7×10^{-7}	1.1×10^{-5}
Total	Adult	1.1×10^{-4}	1.3×10^{-7}	6.6×10^{-8}	7.2×10^{-7}	1.8×10^{-6}	4.8×10^{-5}
Dry season		1.4×10^{-4}	1.7×10^{-7}	8.3×10^{-8}	8.7×10^{-7}	2.3×10^{-6}	6.0×10^{-5}
Wet season		3.3×10^{-5}	3.1×10^{-8}	2.2×10^{-8}	3.0×10^{-7}	4.3×10^{-7}	1.5×10^{-5}

light vehicles (Pereira et al. 2023b), while a ratio of 1.38 was pointed out as typical of crustal materials (He et al. 2008). A mean EC/Cu ratio of 11 was obtained, which is close to that observed in tunnels for LDVs (varying between 5 and 8), whereas values above 80 were reported for emissions from HDVs (Pereira et al. 2023a).

In all the studied periods in Cuiabá (dry and wet seasons) and for the three groups studied, the values obtained for the hazard quotients (HQ) were higher for dermal contact, followed by ingestion and inhalation (Table S4). Hazard quotients for elements were in the following order, for dermal contact $Mn > Cd > Pb > Cu > Ni > Co$, for ingestion $Pb > Cu > Cd > Mn > Co > Ni$, and for inhalation $Mn > Cd > Ni > Co > Cu > Pb$ (Table S4). The non-cancer hazard or risk index (HI) of all quantified elements (Cu, Mn, Pb, Co, Ni, and Cd) was lower than 1, indicating negligible non-carcinogenic risk for residents in Cuiabá (Table 4 and Fig. 5a).

Cancer risks from ingestion, inhalation, and dermal due to exposure to PM_{10} -bound Cu, Cd, Co, Mn, Ni, and Pb are summarized in Table S5. The mean cancer risks by all routes of exposure in PM_{10} for elements are presented in Table S5 and Fig. 5b. The ILCR values for the three exposure routes and the total for all ages were below 10^{-6} and considered insignificant by the US EPA.

PAHs, nitro-PAHs, and oxy-PAHs

On average, the total PAH concentration ($\Sigma PAHs$) was higher in the dry season (39 ng m^{-3}) than in the wet season (29 ng m^{-3}) (Fig. 6). The most abundant compound for both seasons was BkF, representing 16 and 21% of $\Sigma PAHs$, respectively. The second most abundant in the dry season was Chry, with a mean of 5.8 ng m^{-3} , followed by BeP > InP > BbF > DahA. In the wet season, the second most

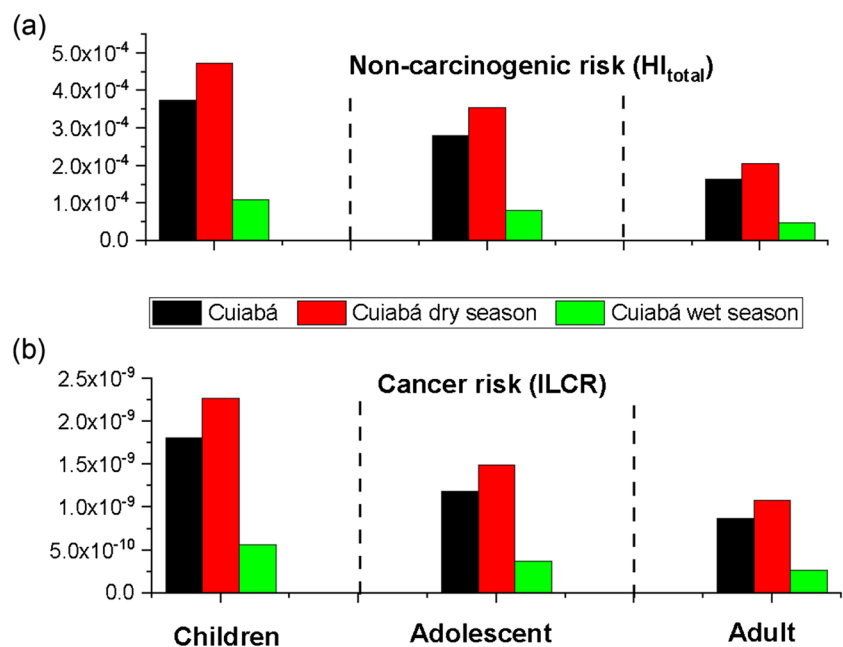
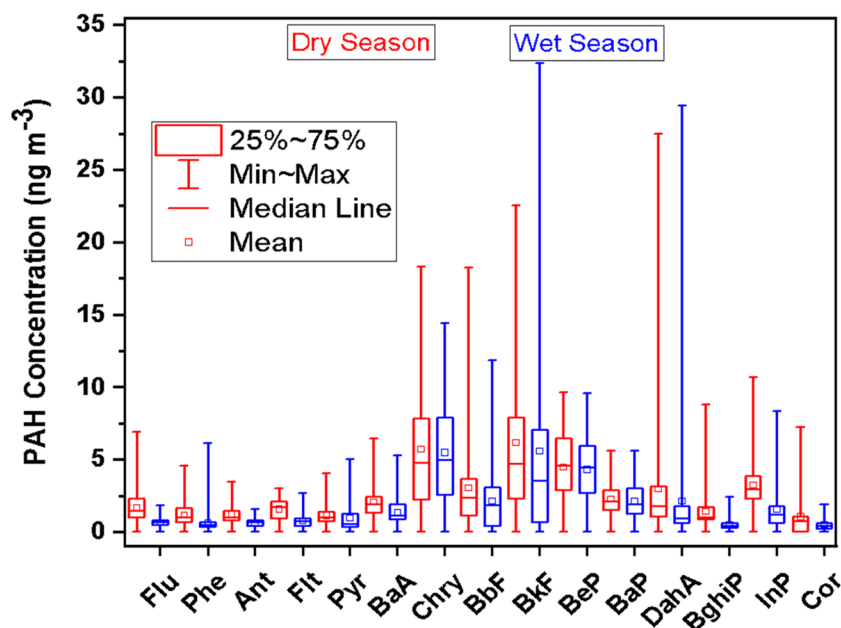
Fig. 5 Cumulative non-carcinogenic risks (HI) and lifetime carcinogenic risks (ILCR) for children, adolescents, and adults

Fig. 6 Concentrations of PAHs studied in the dry and wet seasons



abundant PAH was Chry with a mean of 5.8 ng m^{-3} , followed by BeP, DahA, and InP. Thus, similar profiles were observed for the major compounds in both seasons. Most of them are HMW compounds (except Chry), tend to be concentrated in the particulate phase (Kim et al. 2013) and are dominant in emissions from gasoline-powered LDVs (Pereira et al. 2023a; Ravindra et al. 2008). As observed in a study performed at the Metropolitan Area of São Paulo in 2018, the source profiles of organic carbon were characterized by four-ring PAHs (Chry and Pyr) and five-ring PAHs (BeP and BaP), while in a more HDV-impacted tunnel, higher LMW-PAH abundances were observed (Pyr, Flt, and Phe) (Pereira et al. 2023a, 2023b). Flu, Phe, and Pyr have been documented as major PAHs in emissions from biomass burning, while Chry, DahA, and BaA have been linked to stationary sources (Magalhães et al. 2007).

The largest contributions to total PAHs in both seasons were from 5-ring PAHs (51%), followed by the 4-ring PAHs (28%), while the lowest contributions were from 6- and 3-ring PAHs, accounting for 11% and 10%, respectively. LMW and HMW compounds represented 37% and 63% of Σ PAHs, respectively. This may reflect the predominance of pyrogenic sources (Zhang et al. 2008).

In a study carried out in Porto Velho, a city located in the western Amazon, total concentrations of 3 and 1 ng m^{-3} were observed in the dry and wet seasons (de Oliveira Alves et al. 2015), an order of magnitude lower than those found in the present study. Differences between PAH concentrations may vary according to the sampling site, the geography of the area, the meteorological conditions, and the emission sources. BaA, Chry, BbF, BkF, and BaP were among the most abundant PAHs reported by de Oliveira Alves et al.

(2015). In another study by Vasconcellos et al. (1998) in an Amazon Forest area (Alta Floresta, Mato Grosso), the highest concentrations were obtained for BkF, BeP, BghiP, InP, and Chry.

Table 5 shows the concentration range of the nitro-PAHs investigated. According to previous results, concentrations of nitro-PAHs range from 2 to 1000 times lower than those of their precursor PAHs (Bamford and Baker 2003). 4-NPyr was the species with the highest concentrations all year round, reaching up to 1.2 ng m^{-3} in both seasons. This compound presents greater carcinogenic potential than BaP (IARC 2010). 1-NPyr, which is highly mutagenic (IARC 2010), achieved concentrations up to 0.8 ng m^{-3} . 6-NBaP and 6-NChry, compounds emitted by diesel and gasoline combustion (Ringuet et al. 2012), were also identified.

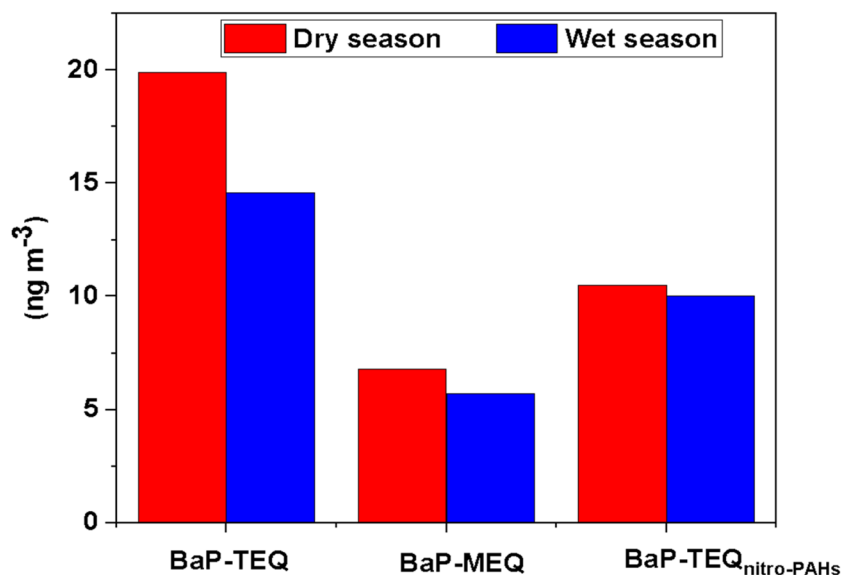
The sum of oxy-PAH was 3.8 ng m^{-3} in the dry season, period during which the highest concentrations were recorded. Of the four oxy-PAH determined, 2-MAQ showed the highest values in both seasons, reaching a peak concentration of 2.4 ng m^{-3} , followed by 9,10-AQ and 9-FO. This compound is suspected of being carcinogenic to humans and is related to biomass burning (Gori et al. 2009). Oxy-PAHs are not uniquely produced during incomplete combustion processes, but are also formed when PAHs undergo photochemical reactions with hydroxyl radicals, nitrate radicals and ozone (de Oliveira Alves et al. 2020; Chen and Zhu 2014; Finlayson-Pitts and Pitts 1999). Higher proportions of oxy-PAHs have also been attributed to the emissions of diesel-powered HDVs in a tunnel study in São Paulo (Pereira et al. 2023a).

Values obtained for BaP-TEQ, BaP-MEQ, and BaP-TEQ_{nitro-PAHs} in the dry and wet seasons for the studied site

Table 5 Range and frequency of detection of PAH derivatives in Cuiabá.

Compound	Season	
	Dry (ng m ⁻³)	Wet
Nitro-PAHs		
2-Flu	0.2–2.2 (94%)	0.6–1.2 (82%)
9-NPhe	0.3–2.9 (95%)	0.2–2.7 (97%)
3-NFlt	0.6–2.7 (93%)	0.4–1.2 (95%)
4-NPyr	0.8–2.4 (94%)	1–1.6 (95%)
1-NPyr	0.4–1.4 (96%)	0.2–1.2 (95%)
6-NChry	0.6–2.2 (88%)	0.7–1.7 (85%)
7-NBaA	0.1–2.6 (100%)	0.6–1.5 (92%)
6-NBaP	0.5–1.7 (94%)	0.3–1.7 (92%)
5-NAce	0.2–1.7 (96%)	0.2–1.1 (92%)
Oxy-PAHs		
9,10-AQ	0.5–1.7 (94%)	0.3–1.7 (92%)
9-FO	0.2–1.7 (96%)	0.3–1.1 (92%)
2-MAQ	0.4–2.3 (98%)	0.2–2.1 (92%)
7,12-BAQ	0.3–1.3 (96%)	0.4–1.1 (95%)

are presented in Fig. 7. Estimated ILCR values for inhalation, dermal, and ingestion exposure routes are shown in Fig. 8. In the whole period, the values were 19, 6, and 10 ng m⁻³ for BaP-TEQ, BaP-MEQ, and BaP-TEQ_{nitro-PAHs}, respectively. The concentrations of BaP-TEQ and BaP-MEQ in the dry season were higher than those in the rainy season, showing significant differences (Mann-Whitney; $p < 0.05$), which can be attributed to climatic conditions less favorable to the dispersion of pollutants and the greater influence of biomass burning. The concentrations of BaP-TEQ_{nitro-PAHs} were similar in both seasons (Mann-Whitney; $p > 0.05$).

Fig. 7 BaP equivalent carcinogenicity and mutagenicity of PAHs and derivatives

The values obtained for BaP_{eq} in this work were higher than those obtained by Gregoris et al. (2014), in an Italian region in 2009 and 2012. The PAHs that most contributed to the calculated BaP equivalents (carcinogenic and mutagenic) were DahA, BaP, and InP, including species more associated with the emissions of LDVs (Pereira et al. 2023a).

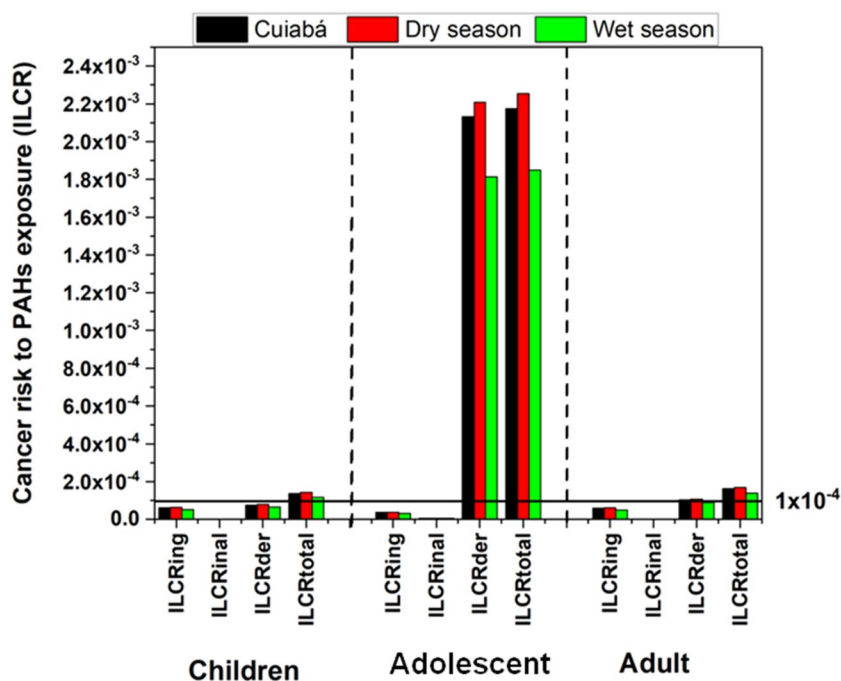
The total ILCR for children, adolescents, and adults were 1.4×10^{-4} , 2.2×10^{-3} , and 1.6×10^{-4} , respectively. Regardless of age, dermal exposure is the route that presents the highest risks. Zhang et al. (2019) classified ILCR $< 1.0 \times 10^{-6}$ as a very low cancer risk, $1.0 \times 10^{-6} < \text{ILCR} < 1.0 \times 10^{-4}$ low risk, $1.0 \times 10^{-4} < \text{ILCR} < 1.0 \times 10^{-3}$ moderate risk, $1.0 \times 10^{-3} < \text{ILCR} < 1.0 \times 10^{-1}$ high risk, and ILCR $> 1.0 \times 10^{-1}$ very high risk.

Total ILCR values were higher in the dry season than in the wet season. Total ILCR values higher than those suggested by the USEPA (1.0×10^{-6} to 1.0×10^{-4}) were recorded in both seasons. This is an indicator that the daily inhalation, ingestion, and dermal contact dose of PAHs bound to PM₁₀ particles and cancer risks for children, adolescents, and adults in Cuiabá are well above tolerable levels. Zhang et al. (2019), in a study in Wuhan (China), reported values much higher than those obtained in this work.

Concentration of n-alkanes

The predominant aliphatic species during the entire period studied were C₂₉ (24 ng m⁻³), C₃₀ (23 ng m⁻³), C₂₈ (23 ng m⁻³), and C₂₇ (19 ng m⁻³). Higher concentrations of long chain odd n-alkanes (C₂₇, C₂₉, C₃₁, and C₃₃) are indicative of emissions from vegetable waxes (Ding et al. 2009; Simoneit et al. 1990), which may be related to biogenic emissions and/or biomass burning (Simoneit 2002). The sum of n-alkanes between C₁₆ and C₂₅ (lighter) was 59 ng m⁻³ (24% of the total), while the heaviest homologs (C₂₆–C₄₀) totaled 179

Fig. 8 Cancer risk due to PAHs exposure in the PM₁₀ collected in the capital of Mato Grosso (Cuiabá)



ng m⁻³ (76% of the total). *n*-Alkanes with lower molecular weight (C₂₀–C₂₆) are more associated with the exhaust of vehicles (Alves et al. 2020). The molecular distribution of the *n*-alkanes investigated here in the dry and wet seasons is shown in Fig. 9.

The concentrations of the homologs followed the same behavior in the two studied seasons, except for C₄₀, whose concentration was, on average, higher in the wet season. C₃₀ was the homolog with highest concentrations in both periods, and the sum of the C₂₆–C₄₀ concentrations was higher in the dry season compared to the rainy period. In the dry season, CPI was 1.4, a value higher than that found in the wet period (1.0). The CPI values were similar to those obtained previously (0.9 and 1.4) in periods of intense and moderate biomass burning, pointing to an increase of biogenic emissions in the wet period (de Oliveira 2014).

Source apportionment

PAH diagnostic ratios

The diagnostic ratio between low and high molecular weight (LMW-PAHs/HMW-PAHs) can be influenced by several factors (pyrogenic and petrogenic sources, diesel and gasoline exhausts, and the gas-particle partition of PAHs). The values obtained for this ratio in the two seasons were below 1, indicating the contribution of pyrogenic sources (Zhang et al. 2008) (Table 5). Lower LMW-PAHs/HMW-PAHs can also be attributed to a higher contribution of gasoline

compared to diesel. The study of Pereira et al. (2023a) found tenfold lower ratios for a gasoline-impacted tunnel (0.7) compared to a diesel and gasoline-impacted road underground infrastructure (7.5). Therefore, the ratios found here reflect mixed contributions from pyrogenic and gasoline exhaust emissions.

Other diagnostic ratios were also studied to assess the main sources of PAHs, such as InP/(InP+BghiP), BaA/(BaA+Chry), Flt/(Flt+Pyr), BaP/BghiP, and Ant/(Ant+Phe) (Table 6). The results for these ratios were similar in both seasons, indicating pyrogenic emissions, corroborating the fact that the urban site is often influenced by biomass burning aerosols.

A parameter that can differentiate the contribution from primary sources is the total index (Eq. 18). It is defined as the sum of some previously calculated diagnostic ratios. A total index (TI) higher than 4 denotes that the PAHs were generated by high-temperature processes (Bootdee et al. 2016).

$$TI = \frac{Flt/(Flt + Pyr)}{0.4} + \frac{Ant/(Ant + Phe)}{0.1} + \frac{BaA/(BaA + Chry)}{0.2} + \frac{InP/(InP + BghiP)}{0.5} \quad (21)$$

The total indexes for the dry (10) and wet (9) seasons in Cuiabá were found to be much higher than 4. This result indicates that PAHs were emitted in high-temperature combustion processes. In general, all the diagnostic ratios studied suggested that coal, wood, and oil burning, as well as vehicular emissions, are the primary sources of particle-bound PAHs in the studied site.

Fig. 9 Concentrations of the studied carbon homologs (n-alkanes)

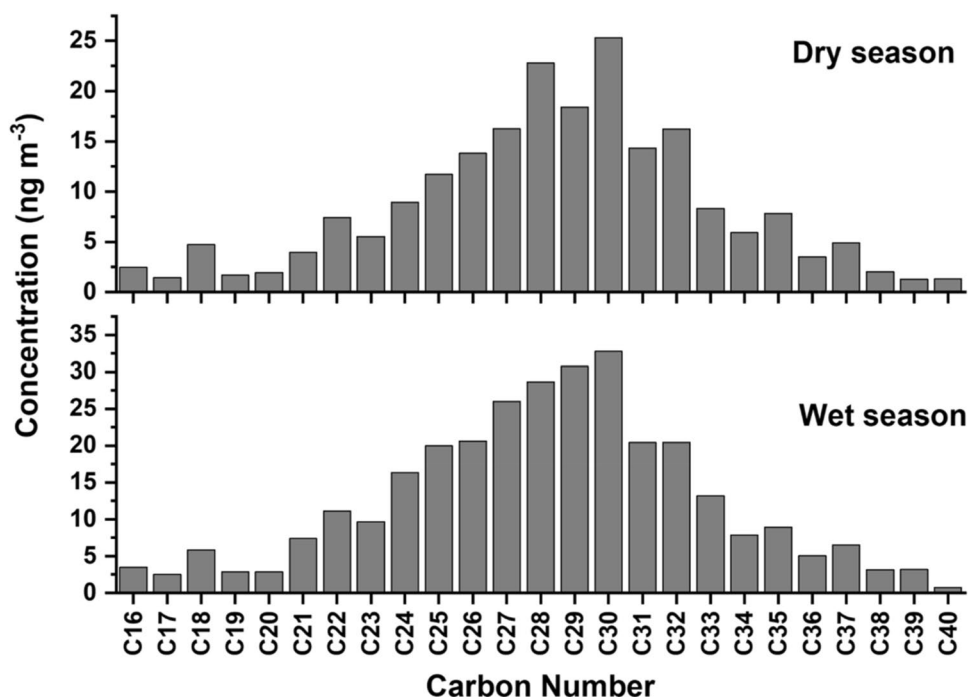


Table 6 Diagnostic molecular reasons for PAHs at the two seasons

Diagnostic	Sources	Reference value	Dry season	Wet season
LMW/HMW ^a	Pyrogenic	< 1	0.6	0.7
	Petrogenic	> 1		
InP/(InP+BghiP) ^{b,c}	Petrogenic	< 0.2	0.7	0.7
	Fossil fuel combustion	0.2 - 0.5		
	Coal, wood, and grass combustion	> 0.5		
BaA/(BaA+Chry) ^{b,d}	Petrogenic	< 0.2	0.3	0.2
	Coal combustion	0.2 - 0.35		
	Vehicle emissions	> 0.35		
Flt/(Flt+Pyr) ^{b,e}	Petrogenic	< 0.4	0.6	0.5
	Fossil fuel combustion	0.4 - 0.5		
	Coal, wood, and grass combustion	> 0.5		
BaP/BghiP ^b	Traffic	< 0.6	2.2	5.4
	Non-traffic	> 0.6		
Ant/(Ant+Phe) ^f	Petrogenic	< 0.1	0.5	0.5
	Pyrogenic	> 0.1		

^aZhang et al. (2008)

^bKatsoyiannis et al. (2011)

^cYunker et al. (2002)

^dAkyüz and Çabuk (2010)

^eRavindra et al. (2008)

^fde la Torre-Roche et al. (2009)

Polar plots and correlations between species

Polar plot graphs were constructed with the concentration values of PM₁₀, OC, EC, water-soluble species, elements, PAHs, and wind speed and direction. Correlations were also

made between the concentrations of the aforementioned species (Figures S2 and S4 (dry season) and Figures S3 and S5 (rainy season)).

OC was correlated with EC in the two seasons ($R^2 = 0.64$ and 0.73). The slightly lower correlation for the wet period

may indicate different emission sources, atmospheric reaction pathways, or removal processes between seasons.

The dry season showed a good correlation between almost all the water-soluble inorganic species that were determined. The low correlation between Na^+ and Cl^- ($R^2 = 0.34$) during the wet season could be explained by the distance of the sampling site from the Atlantic Ocean and by the contribution of Na^+ from sources such as soil and biomass burning (Custodio et al. 2019). Biomass burning is one of the most important sources of Cl^- containing species in the atmosphere (Lobert et al. 1999). In Figures S2 and S3, it can be observed that these species show different wind dependent patterns, and the trajectories of the air masses are mainly from the continent (Figs. 4d, e). Na^+ presented a high correlation with NO_3^- (0.8), which can be related to the formation of NaNO_3 , associated with the depletion of chloride and sea-spray aging (Cesari et al. 2018).

During the two periods studied it was possible to observe moderate to strong correlations between SO_4^{2-} and NO_3^- with EC, OC, K^+ , Na^+ , Ca^{2+} , and Mg^{2+} (Figures S4 and S5). In the dry season, these correlations were higher, pointing to a common origin associated with the same wind direction (Figures S2 and S3). Coarse mode nitrate and sulfate can result from heterogeneous reactions of HNO_3 and H_2SO_4 with alkaline surfaces of soil particles (Tang et al. 2016; Wang et al. 2016). The interaction of SO_2 and concrete or calcareous (e.g., from construction sources) may lead to the formation of sulfate particles containing Ca and Na (Bourotte et al. 2006). During the wet season, NH_4^+ is well correlated with NO_3^- and relatively well correlated with SO_4^{2-} , suggesting an increase in the interaction of NH_3 and HNO_3 in this season (Ianniello et al. 2011). The correlations of secondary formation species appear to be more predominant in the wet season, under higher relative humidity. The formation of sulfate and nitrate in clouds and fog droplets may be related to the heterogeneous aqueous transformation of sulfur and nitrogen oxides under high relative humidity (RH) (Huang et al. 2016). The neutralization of the acids HNO_3 and H_2SO_4 may be rather linked to carbonated minerals since the molar ratio $[\text{NH}_4^+]/[\text{SO}_4^{2-}]$ is much lower than 2.

The correlations between Mg^{2+} and Ca^{2+} were significant in both seasons and presented similar patterns (Figures S2, S3, S4, and S5). These species showed significant correlations with both EC and K^+ , which could indicate that they are emitted by similar sources, probably by the resuspension of soil and biomass burning emissions, that may increase in dry periods (Custodio et al. 2019) and can also have the same removal processes. In the dry season, most of the elements presented high correlations with each other ($r > 0.7$), suggesting similar sources, or sources that increase with similar meteorological conditions. Ca^{2+} was correlated with Mn and Fe, which are present in the crust and also in

vehicular emissions (Pereira et al. 2023a; Lee 1999). These species correlated with EC and OC ($r > 0.7$), suggesting that species anthropogenically emitted can settle onto the soil and then be resuspended along with crustal material.

Depending on the season, PAHs showed different patterns (Figure S2 and S3), especially when lighter PAHs (Flu, Phe, Ant, Flt, and Pyr) are compared with heavier PAHs (InP, DBA, and BghiP). Correlations between PAHs and other species were higher in the dry period than in the wet season, reflecting different emissions sources and meteorological conditions.

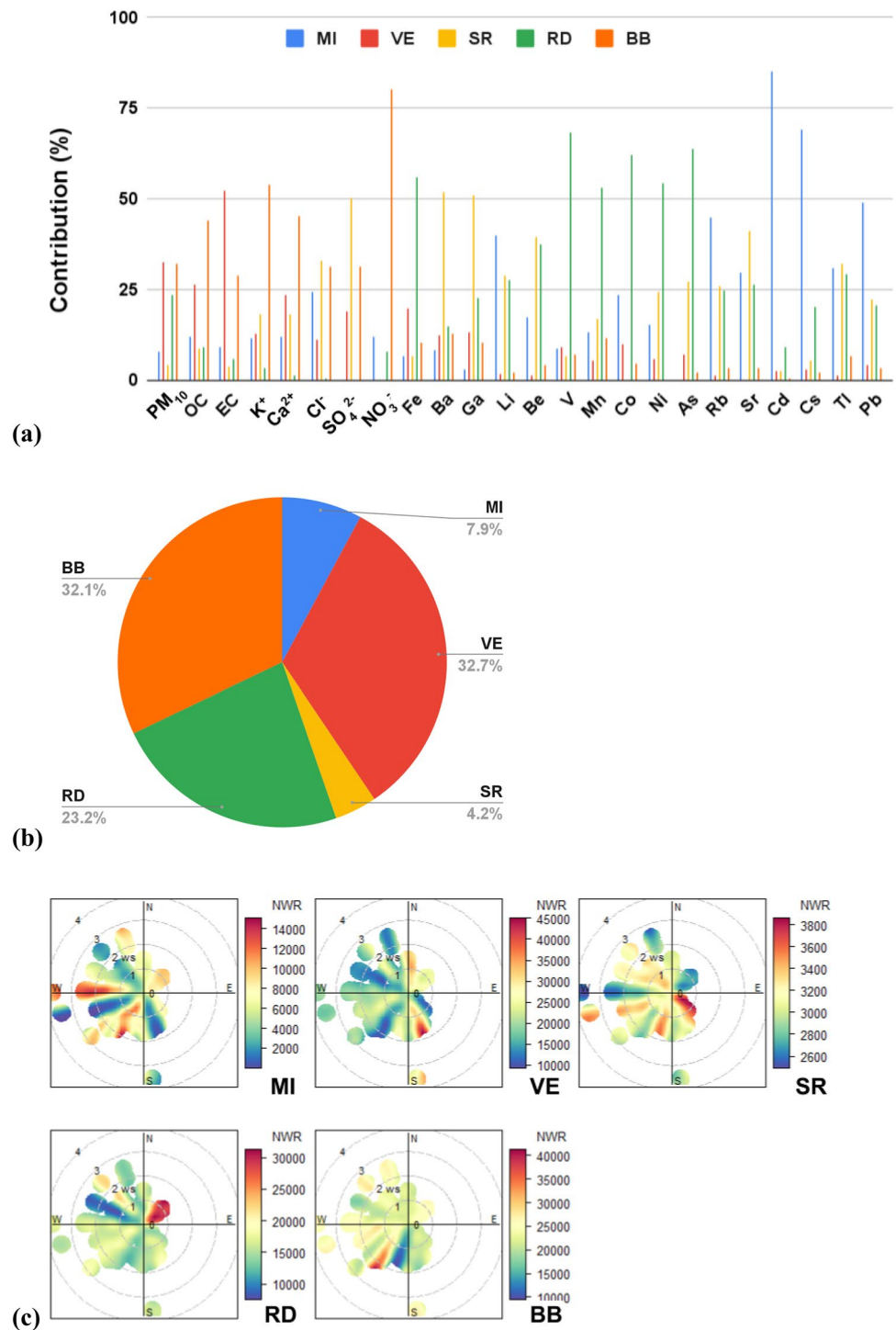
PMF receptor model

Source apportionment of the samples ($n = 120$) was carried out by applying the PMF receptor model. Twenty-two chemical species were set as “strong” variables, vanadium was set as “weak” variable, and the others were set as “bad” and excluded from the model, as recommended by Paatero and Tapper (1994). The concentration of PM_{10} particulate material was set as the total variable. Three- to eight-factor runs were made, with the five-factor run presenting the best results (base model displacement and bootstrap method, Tables S6 and S7). Extra uncertainties of 5% were added to avoid the discard of poor-quality data, as reported by Paatero and Hopke (2003). Profiles of the source contributions (%) to PM_{10} obtained in the PMF analyses and the polar plots and seasonal distribution of the PMF factor contributions are shown in Fig. 10.

Factor 1 contributed to only 8% of PM_{10} and presented loadings of Cd, Cs, and lesser amounts of Pb, Rb, and Li. As, Cd, and Pb have been related to mining activities (Csavina et al. 2011). High Li, Sr, and Rb loading have been previously linked to urban works (Amato et al. 2009). Thus, this factor seems to be related to mining or dust generating activities (e.g., urban works) (MI), it increases with winds coming from areas in the outskirts with exposed soil and constructions (west) and mining areas in the surroundings (northeast), although it also increases with winds coming from the city center (south). This influence should be further investigated.

Factor 2 was one of the most dominant and was attributed to vehicular exhaust (VE), presenting loadings of great amounts of OC and EC, and also relatively lower amounts of Ca^{2+} , SO_4^{2-} , Fe, Ba, Ga, and V. It accounted for 33% of the PM_{10} concentrations, increasing with southwestern winds that passed through the downtown area. Factor 3 is not clear, as it may be related to soil resuspension (SR) due to the presence of species found in trace amounts as Ba, Sr, Li, and Rb (Calvo et al. 2013), but also presents SO_4^{2-} , which is mostly related to secondary formation and may be due to the reaction of secondarily produced H_2SO_4 and the carbonated minerals in the soil; however, barium is often found in the abrasion of

Fig. 10 PMF factor source profiles (a), contributions to PM_{10} (b), and polar plots (c)



brake pads (Thorpe and Harrison 2008). This factor accounts for only 4% of PM_{10} and increases with winds coming from the southeast.

Factor 4 was related to road dust resuspended by traffic (RD), accounting for 23% of PM_{10} . It included species emitted in the exhaust of vehicle tailpipes, as well as in particles from brake and tire wear (non-exhaust emissions), such as Fe, V, Mn, Ni, and As (Pant and Harrison 2013). Additionally,

species related to road dust resuspension, such as Sr, and Rb, were also part of factor 4. OC and EC were more associated with Factor 2, rather than Factor 4, which may suggest lower vehicle exhaust component in the latter. This factor contribution increases with winds coming from the northeast, where there is a main road connecting to the outskirts.

Factor 5 was associated with biomass burning (BB) due to the presence of K^+ and OC, however nitrate was also found.

NO_3^- and K^+ have been associated with biomass burning plumes in the Amazon area (Gonçalves et al. 2016). Potassium and nitrate was also related to agricultural activities in the state of São Paulo (Allen et al., 2010). Nitrate may also be related to NO formed in the burning conditions (Vicente et al. 2013). The presence of calcium suggests that it is also mixed with a soil source (Pereira et al. 2017). It accounted for 32% of PM_{10} and together with vehicular emissions were major sources. Combustion sources as those may play an important role in both oxidative stress and genotoxicity (Guascito et al. 2023). Differently from what was observed in studies performed in São Paulo, it was not possible to observe a separated secondary formation factor (Serafeim et al. 2023; Pereira et al. 2017). NO_3^- and SO_4^{2-} are likely more related to soil resuspension in the present study as HNO_3 and H_2SO_4 may react with carbonated minerals in the soil, as pointed in “Polar plots and correlations between species.” No industrial sources were identified; this type of source is difficult to be quantified by receptor models, with a high variability (Belis et al. 2020).

Conclusions

This study presented the results obtained for the concentration of PM_{10} and its chemical characterization, which includes different classes of compounds such as OC, EC, WSII, PAHs and derivatives, and n-alkanes in a region impacted by biomass burning, traffic emissions, and industrial and agricultural activities. Higher concentrations of OC, EC, and WSII were registered in the dry season, possibly due to biomass burning. PAHs, nitro-PAHs, and oxy-PAHs showed a similar behavior in the dry and rainy seasons. However, the concentrations were higher in the dry season, during which molecular weight compounds predominated. For n-alkanes, there were no significant differences between seasons. According to the results of PAH diagnostic indices and the correlations between all determined species, the main pollutant emissions sources were biomass burning (wood, coal, and grass), vehicles, and soil resuspension. The lifetime cancer risks (inhalation, dermal, and ingestion) due to PAHs' exposure estimated for the two seasons far exceeded the value stipulated by the WHO, showing that children, adolescents, and adults in Cuiabá are exposed to concentrations well above the tolerable levels. The results shown by the PMF model pointed to biomass burning and vehicular emissions as the major sources of PM_{10} . This work provides knowledge about the sources of aerosols in a less studied region highly impacted by anthropogenic activities, which often presents high carcinogenic and mutagenic potential risks for human health, especially for the most vulnerable groups.

Supplementary Information The online version contains supplementary material available at <https://doi.org/10.1007/s11869-023-01467-1>.

Acknowledgements The authors acknowledge the Ministry of the Environment of the State of Mato Grosso (SEMA) for the samples (especially to Sérgio Batista de Figueiredo).

Funding Yendry Jomolca Parra thanks CNPq (project: 155685 / 2016-3, Project 870031 / 2003-1) for the grants. Guilherme M. Pereira thanks FAPESP for grants #16/18438-0, #18/07848-9, and 19/01316-8. The financial support to CESAM by FCT/MCTES (UIDP/50017/2020+UIDB/50017/2020+ LA/P/0094/2020), through national funds, is also acknowledged. Pérola C. Vasconcellos thanks CNPq (grants 301503/2018-4).

Data Availability The datasets generated during and/or analyzed during the current study are available upon request.

Declarations

Ethics approval and consent to participate Not applicable.

Consent for publication Not applicable.

Competing interests The authors declare no competing interests.

References

- Akyüz M, Çabuk H (2010) Gas-particle partitioning and seasonal variation of polycyclic aromatic hydrocarbons in the atmosphere of Zonguldak, Turkey. *Sci Total Environ* 408:5550–5558. <https://doi.org/10.1016/j.scitotenv.2010.07.063>
- Allen AG, Cardoso AA, Wiatr A, Machado CMD, Paterlini WC, Baker J (2010) Influence of intensive agriculture on dry deposition of aerosol nutrients. *J Braz Chem Soc* 21:87–97. <https://doi.org/10.1590/S0103-50532010000100014>
- Alves CA, Evtuygina M, Vicente AMP, Vicente ED, Nunes TV, Silva PMA, Duarte MAC, Pio CA, Amato F, Querol X (2018) Chemical profiling of PM_{10} from urban road dust. *Sci Total Environ* 634:41–51. <https://doi.org/10.1016/j.scitotenv.2018.03.338>
- Alves CA, Gomes J, Nunes T, Duarte M, Calvo A, Custódio D, Pio C, Karanasiou A, Querol X (2015) Size-segregated particulate matter and gaseous emissions from motor vehicles in a road tunnel. *Atmos Res* 153:134–144. <https://doi.org/10.1016/j.atmosres.2014.08.002>
- Alves CA, Vicente AMP, Calvo AI, Baumgardner D, Amato F, Querol X, Pio C, Gustafsson M (2020) Physical and chemical properties of non-exhaust particles generated from wear between pavements and tyres. *Atmos Environ* 224:117252. <https://doi.org/10.1016/j.atmosenv.2019.117252>
- Amato F, Alastuey A, Karanasiou A, Lucarelli F, Nava S, Calzolari G, Severi M, Becagli S, Gianelle VL, Colombi C, Alves C, Custódio D, Nune T, Cerqueira M, Pio C, Eleftheriadis K, Diapouli E, Reche C, Minguillón MC et al (2016) AIRUSE-LIFE+: a harmonized PM speciation and source apportionment in five southern European cities. *Atmos Chem Phys* 16:3289–3309. <https://doi.org/10.5194/acp-16-3289-2016>
- Amato F, Pandolfi M, Escrig A, Querol X, Alastuey A, Pey J, Perez N, Hopke PK (2009) Quantifying road dust resuspension in urban environment by Multilinear Engine: A comparison with PMF2. *Atmos Environ* 43:2770–2780. <https://doi.org/10.1016/j.atmosenv.2009.02.039>
- Artaxo P, Martins JV, Yamasoe MA, Procópio AS, Pauliquevis TM, Andreae MO, Guyon P, Gatti LV, Leal AMC (2002) Physical and chemical properties of aerosols in the wet and dry seasons in

- Rondônia, Amazonia. *J Geophys Res D Atmos* 107:1–14. <https://doi.org/10.1029/2001JD000666>
- Artaxo P, Rizzo LV, Brito JF, Barbosa HMJ, Arana A, Sena ET, Cirino GG, Bastos W, Martin ST, Andreae MO (2013) Atmospheric aerosols in Amazonia and land use change: From natural biogenic to biomass burning conditions. *Faraday Discuss* 165:203–235. <https://doi.org/10.1039/c3fd00052d>
- Bamford HA, Baker JE (2003) Nitro-polycyclic aromatic hydrocarbon concentrations and sources in urban and suburban atmospheres of the Mid-Atlantic region. *Atmos Environ* 37:2077–2091. [https://doi.org/10.1016/S1352-2310\(03\)00102-X](https://doi.org/10.1016/S1352-2310(03)00102-X)
- Behera SN, Cheng J, Huang X, Zhu Q, Liu P, Balasubramanian R (2015) Chemical composition and acidity of size-fractionated inorganic aerosols of 2013–14 winter haze in Shanghai and associated health risk of toxic elements. *Atmos Environ* 122:259–271. <https://doi.org/10.1016/j.atmosenv.2015.09.053>
- Belis CA, Pernigotti D, Pirovano G, Favez O, Jaffredo JL, Kuenen J, Denier van Der Gon H, Reizer M, Riffault V, Alleman LY, Almeida M, Amato F, Angyal A, Argyropoulos G, Bande S, Beslic I, Besombes JL, Bove MC, Broto P et al (2020) Evaluation of receptor and chemical transport models for PM₁₀ source apportionment. *Atmos. Environ. X* 5:100053. <https://doi.org/10.1016/j.aeaoa.2019.100053>
- Boonyatumanond R, Murakami M, Wattayakorn G, Togo A, Takada H (2007) Sources of polycyclic aromatic hydrocarbons (PAHs) in street dust in a tropical Asian mega-city, Bangkok, Thailand. *Sci Total Environ* 384:420–432. <https://doi.org/10.1016/j.scitotenv.2007.06.046>
- Bootdee S, Chantara S, Prapamontol T (2016) Determination of PM_{2.5} and polycyclic aromatic hydrocarbons from incense burning emission at shrine for health risk assessment. *Atmos Pollut Res* 7:680–689. <https://doi.org/10.1016/j.apr.2016.03.002>
- Bourotte C, Forti MC, Melfi AJ, Lucas Y (2006) Morphology and solutes content of atmospheric particles in an urban and a natural area of São Paulo State, Brazil. *Water Air Soil Pollut* 170:301–316. <https://doi.org/10.1007/s11270-005-9001-1>
- Brito J, Rizzo LV, Herckes P, Vasconcellos PC, Caumo SES, Fornaro A, Ynoue RY, Artaxo P, Andrade MF (2013) Physical–chemical characterisation of the particulate matter inside two road tunnels in the São Paulo Metropolitan Area. *Atmos Chem Phys* 13:12199–12213. <https://doi.org/10.5194/acp-13-12199-2013>
- Calvo AI, ER TLA, Alves C, Nunes T, Duarte M, Coz E, Custodio D, Castro A, Artiñano B, Fraile R (2013) Particulate emissions from the co-combustion of forest biomass and sewage sludge in a bubbling fluidised bed reactor. *Fuel Process Technol* 114:58–68. <https://doi.org/10.1016/j.fuproc.2013.03.021>
- Candeias C, Vicente E, Tomé M, Rocha F, Ávila P, Alves C (2020) Geochemical, mineralogical and morphological characterisation of road dust and associated health risks. *Int J Environ Res Public Health* 17:1563. <https://doi.org/10.3390/ijerph17051563>
- Cao F, Zhang YX, Lin X, Zhang YL (2021) Characteristics and source apportionment of non-polar organic compounds in PM_{2.5} from the three megacities in Yangtze River Delta region, China. *Atmos Res* 252:105443. <https://doi.org/10.1016/j.atmosres.2020.105443>
- Castanho ADA, Artaxo P (2001) Wintertime and summertime São Paulo aerosol source apportionment study. *Atmos Environ* 35:4889–4902. [https://doi.org/10.1016/S1352-2310\(01\)00357-0](https://doi.org/10.1016/S1352-2310(01)00357-0)
- Caumo S (2020) Caracterização química e determinação do potencial oxidativo em material particulado atmosférico coletado perto de uma área industrial na região metropolitana de São Paulo. Doctoral Thesis, University of São Paulo, Brazil. <https://doi.org/10.11606/T.46.2020.tde-02122022-172743>
- Caumo S, Vicente A, Custódio D, Alves C, Vasconcellos P (2018) Organic compounds in particulate and gaseous phase collected in the neighbourhood of an industrial complex in São Paulo (Brazil). *Air Qual Atmos Heal* 11:271–283. <https://doi.org/10.1007/s11869-017-0531-7>
- Cesari D, De Benedetto GE, Bonasoni P, Busetto M, Dinioi A, Merico E, Chirizzi D, Cristofanelli P, Donato A, Grasso FM, Marinoni A, Pennetta A, Contini D (2018) Seasonal variability of PM_{2.5} and PM₁₀ composition and sources in an urban background site in Southern Italy. *Sci Total Environ* 612:202–213. <https://doi.org/10.1016/j.scitotenv.2017.08.230>
- Chen W, Zhu T (2014) Formation of nitroanthracene and anthraquinone from the heterogeneous reaction between NO₂ and anthracene adsorbed on NaCl particles. *Environ Sci Technol* 48:8671–8678. <https://doi.org/10.1021/es501543g>
- CONAMA (2018). RESOLUÇÃO CONAMA Nº 491 DE 19/11/2018. <http://www2.mma.gov.br/port/conama/legiabre.cfm?codlegi=740>. Accessed 23 July 2020.
- Csavana J, Landázuri A, Wonaschütz A, Rine K, Rheinheimer P, Barbaris B, Conant W, Sáez AE, Betterton EA (2011) Metal and metalloid contaminants in atmospheric aerosols from mining operations. *Water Air Soil Pollut* 221:145–157. <https://doi.org/10.1007/s11270-011-0777-x>
- Custódio D, Alves C, Jomolca Y, Vasconcellos PC (2019) Carbonaceous components and major ions in PM₁₀ from the Amazonian Basin. *Atmos Res* 215:75–84. <https://doi.org/10.1016/j.atmosres.2018.08.011>
- Custódio D, Cerqueira M, Alves C, Nunes T, Pio C, Esteves V, Frosini D, Lucarelli F, Querol X (2016) A one-year record of carbonaceous components and major ions in aerosols from an urban kerbside location in Oporto, Portugal. *Sci Total Environ* 562:822–833. <https://doi.org/10.1016/j.scitotenv.2016.04.012>
- Custódio D, Pinho I, Cerqueira M, Nunes T, Pio C (2014) Indoor and outdoor suspended particulate matter and associated carbonaceous species at residential homes in northwestern Portugal. *Sci Total Environ* 473–474:72–76. <https://doi.org/10.1016/j.scitotenv.2013.12.009>
- de Cavalcanti IFA, Ferreira NJ, Silva MGA, da Dias MAFS (2009) Tempo e clima no Brasil. Oficina de Textos, São Paulo
- de la Torre-Roche RJ, Lee WY, Campos-Díaz SI (2009) Soil-borne polycyclic aromatic hydrocarbons in El Paso, Texas: analysis of a potential problem in the United States/Mexico border region. *J Hazard Mater* 163:946–958. <https://doi.org/10.1016/j.jhazmat.2008.07.089>
- de Oliveira AN (2014) Os efeitos das queimadas na Amazônia em nível celular e molecular. (2014). 133f. Tese (Doutorado em Bioquímica) - Centro de Biotecnologias, Universidade Federal do Rio Grande do Norte, Natal, 2014. Brasil. <https://repositorio.ufrn.br/jspui/handle/123456789/19442>
- de Oliveira AN, Brito J, Caumo S, Arana A, de Souza HS, Artaxo P, Hillamo R, Teinilä K, Medeiros SRB, Vasconcellos PC (2015) Biomass burning in the Amazon region: aerosol source apportionment and associated health risk assessment. *Atmos Environ* 120:277–285. <https://doi.org/10.1016/j.atmosenv.2015.08.059>
- de Oliveira AN, Pereira GM, Di Domenico M, Costanzo G, Benevenuto S, de Oliveira Fonoff AM, de Souza Xavier Costa N, Ribeiro Júnior G, Satoru Kajitani G, Cestari Moreno N, Fotoran W, Iannicelli Torres J, de Andrade JB, Matera Veras M, Artaxo P, Menck CFM, Vasconcellos PC, Saldiva P (2020) Inflammation response, oxidative stress and DNA damage caused by urban air pollution exposure increase in the lack of DNA repair XPC protein. *Environ Int* 145:106150. <https://doi.org/10.1016/j.envint.2020.106150>
- de Oliveira Galvão MF, de Oliveira AN, Ferreira PA, Caumo S, Vasconcellos PC, Artaxo P, de Souza HS, Roubicek DA, Batistuzzo de Medeiros SR (2018) Biomass burning particles in the Brazilian Amazon region: mutagenic effects of nitro and oxy-PAHs and assessment of health risks. *Environ Pollut* 233:960–970. <https://doi.org/10.1016/j.envpol.2017.09.068>

- Ding LC, Ke F, Wang DKW, Dann T, Austin CC (2009) A new direct thermal desorption-GC/MS method: organic speciation of ambient particulate matter collected in Golden, BC. *Atmos Environ* 43:4894–4902. <https://doi.org/10.1016/j.atmosenv.2009.07.016>
- Ding X, Qi J, Meng X (2019) Characteristics and sources of organic carbon in coastal and marine atmospheric particulates over East China. *Atmos Res* 228:281–291. <https://doi.org/10.1016/j.atmosres.2019.06.015>
- Draxler RR, Hess GD (1998) An overview of the HYSPLIT_4 modelling system for trajectories, dispersion and deposition. *Aust Meteorol Mag* 47:295–308
- Durant JL, Busby WF, Lafleur AL, Penman BW, Crespi CL (1996) Human cell mutagenicity of oxygenated, nitrated and unsubstituted polycyclic aromatic hydrocarbons associated with urban aerosols. *Mutat Res - Genet Toxicol* 371:123–157. [https://doi.org/10.1016/S0165-1218\(96\)90103-2](https://doi.org/10.1016/S0165-1218(96)90103-2)
- EPA (1993) Provisional guidance for quantitative risk assessment of polycyclic aromatic hydrocarbons. EPA/600/R-93/089. US Environmental Protection Agency, Cincinnati. <https://rais.ornl.gov/documents/600R93089.pdf>
- EPA (2011) Exposure factors handbook: 2011 edition. U.S. Environ. Prot. Agency EPA/600/R-, 1–1466. EPA/600/R-090/052F. https://edisciplinas.usp.br/pluginfile.php/7049865/mod_resource/content/1/efh-complete%20Exposure%20factors%20handbook%202011%20%281%29.pdf
- EPA (2023). Regional Screening Levels (RSLs) - Generic Tables [WWW Document]. URL <https://www.epa.gov/risk/regional-screening-levels-rsls-generic-tables>
- Fajersztajn L, Saldiva P, Pereira LAA, Leite VF, Buehler AM (2017) Short-term effects of fine particulate matter pollution on daily health events in Latin America: a systematic review and meta-analysis. *Int J Public Health* 62(7):729–738. <https://doi.org/10.1007/s00038-017-0960-y>
- FAO (2022). Food and Agriculture Organization of the United Nations. Countries – select all; regions – world + (total); elements – production quantity; items – soybeans; Years – 2020 + 2019 + 2018 + 2017 + 2016. Available at: <https://www.fao.org/faostat/en/#data/QCL> 11 June 2022.
- Ferreira da Silva M, de Assunção JV, Andrade MF, Pesquero CR (2010) Characterization of metal and trace element contents of particulate matter (PM₁₀) emitted by vehicles running on Brazilian fuels-hydrated ethanol and gasoline with 22% of anhydrous ethanol. *J Toxicol Environ Heal - Part A Curr Issues* 73:901–909. <https://doi.org/10.1080/15287391003744849>
- Finlayson-Pitts BJ, Pitts JN (1999) Chemistry of the upper and lower atmosphere. Academic Press, San Diego. <https://doi.org/10.1016/B978-0-12-257060-5.X5000-X>
- Fu FF, Watanabe K, Yabuki S, Akagi T (2004) Seasonal characteristic of chemical compositions of the atmospheric aerosols collected in urban seaside area at Tokaimura. Eastern Central Japan. *J Geophys Res* 109:D20212. <https://doi.org/10.1029/2004JD004712>
- Gao H, Bai J, Xiao R, Liu P, Jiang W, Wang J (2013) Levels, sources and risk assessment of trace elements in wetland soils of a typical shallow freshwater lake, China. *Stoch Environ Res Risk Assess* 27:275–284. <https://doi.org/10.1007/s00477-012-0587-8>
- Gonçalves C, Figueiredo BR, Alves CA, Cardoso AA, da Silva R, Kanzawa SH, Vicente AM (2016) Chemical characterisation of total suspended particulate matter from a remote area in Amazonia. *Atmos Res* 182:102–113. <https://doi.org/10.1016/j.atmosres.2016.07.027>
- Gori G, Carrieri M, Scapellato ML, Parvoli G, Ferrara D, Rella R, Sturaro A, Bartolucci GB (2009) 2-Methylanthraquinone as a marker of occupational exposure to teak wood dust in boatyards. *Ann Occup Hyg* 53:27–32. <https://doi.org/10.1093/annhyg/men069>
- Goudarzi G, Baboli Z, Moslemnia M, Tobekhak M, Tahmasebi Birgani Y, Neisi A, Ghanemi K, Babaei AA, Hashemzadeh B, Ahmadi Angali K, Dobaradaran S, Ramezani Z, Hassanzadeh MS, Dehdari Rad H, Kayedi N (2021). Assessment of incremental lifetime cancer risks of ambient air PM₁₀-bound PAHs in oil-rich cities of Iran. *J Environ Heal Sci Eng* 19:319–330. <https://doi.org/10.1007/s40201-020-00605-6>
- Gregoris E, Argiriadis E, Vecchiato M, Zambon S, De Pieri S, Donato A, Contini D, Piazza R, Barbante C, Gambaro A (2014) Gas-particle distributions, sources and health effects of polycyclic aromatic hydrocarbons (PAHs), polychlorinated biphenyls (PCBs) and polychlorinated naphthalenes (PCNs) in Venice aerosols. *Sci Total Environ*. 476–477:393–405. <https://doi.org/10.1016/j.scitotenv.2014.01.036>
- Guascito MR, Lionetto MG, Mazzotta F, Conte M, Giordano ME, Caricato R, De Bartolomeo AR, Dinoi A, Cesari D, Merico E, Mazzotta L, Contini D (2023) Characterisation of the correlations between oxidative potential and in vitro biological effects of PM₁₀ at three sites in the central Mediterranean. *J. Hazard. Mater.* 448:130872. <https://doi.org/10.1016/j.jhazmat.2023.130872>
- Gurjar BR, Jain A, Sharma A, Agarwal A, Gupta P, Nagpure AS, Lelieveld J (2010) Human health risks in megacities due to air pollution. *Atmos Environ* 44:4606–4613. <https://doi.org/10.1016/j.atmosenv.2010.08.011>
- He L-Y, Hu M, Zhang Y-H, Huang X-F, Yao T-T (2008) Fine particle emissions from on-road vehicles in the Zhujiang Tunnel, China. *Environ Sci Technol* 42:4461–4466. <https://doi.org/10.1021/es7022658>
- Hedberg E, Gidhagen L, Johansson C (2005) Source contributions to PM₁₀ and arsenic concentrations in Central Chile using positive matrix factorization. *Atmos Environ* 39:549–561. <https://doi.org/10.1016/j.atmosenv.2004.11.001>
- Hu X, Zhang Y, Ding Z, Wang T, Lian H, Sun Y, Wu J (2012) Bioaccessibility and health risk of arsenic and heavy metals (Cd, Co, Cr, Cu, Ni, Pb, Zn and Mn) in TSP and PM_{2.5} in Nanjing, China. *Atmos Environ* 57:146–152. <https://doi.org/10.1016/j.atmosenv.2012.04.056>
- Huang X, Liu Z, Zhang J, Wen T, Ji D, Wang Y (2016) Seasonal variation and secondary formation of size-segregated aerosol water-soluble inorganic ions during pollution episodes in Beijing. *Atmos Res* 168:70–79. <https://doi.org/10.1016/j.atmosres.2015.08.021>
- Ianniello A, Spataro F, Esposito G, Allegrini I, Hu M, Zhu T (2011) Chemical characteristics of inorganic ammonium salts in PM_{2.5} in the atmosphere of Beijing (China). *Atmos Chem Phys* 11:10803–10822. <https://doi.org/10.5194/acp-11-10803-2011>
- IARC (2010) Monographs on the evaluation of carcinogenic risks to humans. IARC Monogr. Eval Carcinog. Risks to Humans 94:9–38
- INPE (2022) Queimadas. Monitoramento de focos ativos por estados: Mato Grosso [WWW Document]. URL https://queimadas.dgi.inpe.br/queimadas/portal-static/estatisticas_estados/. Accessed 4.21.22
- Jadoon WA, Abdel-Dayem SMMA, Saqib Z, Takeda K, Sakugawa H, Hussain M, Shah GM, Rehman W, Syed JH (2020) Heavy metals in urban dusts from Alexandria and Kafr El-Sheikh Egypt: implications for human health. *Environ Sci Pollut Res* 28(2):2007–2018. <https://doi.org/10.1007/s11356-020-08786-1>
- Jadoon WA, Khpalkwak W, Chidya RCG, Abdel-Dayem SMMA, Takeda K, Makhdoom MA, Sakugawa H (2018) Evaluation of levels, sources and health hazards of road-dust associated toxic metals in Jalalabad and Kabul Cities, Afghanistan. *Arch Environ Contam Toxicol* 74:32–45. <https://doi.org/10.1007/s00244-017-0475-9>
- Jung KH, Yan B, Chillrud SN, Perera FP, Whyatt R, Camann D, Kinney PL, Miller RL (2010) Assessment of benzo(a)pyrene-equivalent carcinogenicity and mutagenicity of residential indoor versus outdoor polycyclic aromatic hydrocarbons exposing young

- children in New York city. *Int J Environ Res Public Health* 7:1889–1900. <https://doi.org/10.3390/ijerph7051889>
- Katsoyiannis A, Sweetman AJ, Jones KC (2011) PAH molecular diagnostic ratios applied to atmospheric sources: a critical evaluation using two decades of source inventory and air concentration data from the UK. *Environ Sci Technol* 45:8897–8906. <https://doi.org/10.1021/es202277u>
- Kim KH, Jahan SA, Kabir E, Brown RJC (2013) A review of airborne polycyclic aromatic hydrocarbons (PAHs) and their human health effects. *Environ Int* 60:71–80. <https://doi.org/10.1016/j.envint.2013.07.019>
- Křůmal K, Mikuška P, Večeřa Z (2013) Polycyclic aromatic hydrocarbons and hopanes in PM₁ aerosols in urban areas. *Atmos Environ* 67:27–37. <https://doi.org/10.1016/j.atmosenv.2012.10.033>
- La Colla NS, Botté SE, Marcovecchio JE (2021) Atmospheric particulate pollution in South American megacities. *Environ Rev* 29:415–429. <https://doi.org/10.1139/er-2020-0105>
- Lee JD (1999) *Concise inorganic chemistry*, 5th edn. Wiley, USA
- Liu L, Cheng Y, Wang S, Wei C, Pöhlker ML, Pöhlker C, Artaxo P, Shrivastava M, Andreae MO, Pöschl U, Su H (2020) Impact of biomass burning aerosols on radiation, clouds, and precipitation over the Amazon: relative importance of aerosol-cloud and aerosol-radiation interactions. *Atmos Chem Phys* 20:13283–13301. <https://doi.org/10.5194/acp-20-13283-2020>
- Lober JM, Keene WC, Logan JA, Yevich R (1999) Global chlorine emissions from biomass burning: reactive chlorine emissions. *J Geophys Res* 104:8373–8389. <https://doi.org/10.1016/10.1029/1998JD100077>
- Maenhaut W, Fernández-Jiménez MT, Rajta I, Artaxo P (2002) Two-year study of atmospheric aerosols in Alta Floresta, Brazil: multielemental composition and source apportionment. *Nucl Instruments Methods Phys Res Sect B Beam Interact with Mater Atoms* 189:243–248. [https://doi.org/10.1016/S0168-583X\(01\)01050-3](https://doi.org/10.1016/S0168-583X(01)01050-3)
- Magalhães D, Bruns RE, Vasconcellos PC (2007) Hidrocarbonetos policíclicos aromáticos como traçadores da queima de cana-de-açúcar: uma abordagem estatística. *Quim Nova* 30:577–581. <https://doi.org/10.1590/s0100-40422007000300014>
- Martin ST, Andreae MO, Artaxo P, Baumgardner D, Chen Q, Goldstein AH, Guenther A, Heald CL, Mayol-Bracero OL, McMurry PH, Pauliquevis T, Pöschl U, Prather KA, Roberts GC, Saleska SR, Silva Dias MA, Spracklen DV, Swietlicki E, Trebs I (2010) Sources and properties of Amazonian aerosol particles. *Rev Geophys* 48. <https://doi.org/10.1029/2008RG000280>
- Massimi L, Simonetti G, Buiarelli G, Di Filippo P, Pomata D, Riccardi C, Ristorini M, Astolfi ML, Canepari S (2020) Spatial distribution of levoglucosan and alternative biomass burning tracers in atmospheric aerosols, in an urban and industrial hot-spot of Central Italy. *Atmos Res* 239:104904. <https://doi.org/10.1016/j.atmosres.2020.104904>
- Men C, Liu R, Xu F, Wang Q, Guo L, Shen Z (2018) Pollution characteristics, risk assessment, and source apportionment of heavy metals in road dust in Beijing, China. *Sci Total Environ* 612:138–147. <https://doi.org/10.1016/j.scitotenv.2017.08.123>
- Minnesota Department of Health (2016). Guidance for evaluating the cancer potency of PAH mixture in environmental samples. <https://www.health.state.mn.us/communities/environment/risk/docs/guidance/pahguidance.pdf.%20Accessed%2001%20July%202020>. Accessed 01 June 2020.
- Myhre CL (2013) Aerosols and their relation to global climate and climate sensitivity. *Nat Edu Knowl* 4(5):7
- Nisbet ICT, LaGoy PK (1992) Toxic equivalency factors (TEFs) for polycyclic aromatic hydrocarbons (PAHs). *Regul Toxicol Pharmacol* 16:290–300. [https://doi.org/10.1016/0273-2300\(92\)90009-X](https://doi.org/10.1016/0273-2300(92)90009-X)
- Oliveira C, Martins N, Tavares J, Pio C, Cerqueira M, Matos M, Silva H, Oliveira C, Camões F (2011) Size distribution of polycyclic aromatic hydrocarbons in a roadway tunnel in Lisbon, Portugal. *Chemosphere* 83:1588–1596. <https://doi.org/10.1016/j.chemosphere.2011.01.011>
- Othman M, Latif MT, Jamhari AA, Abd Hamid HH, Uning R, Khan MF, Mohd Nadzir MS, Sahani M, Abdul Wahab MI, Chan KM (2021) Spatial distribution of fine and coarse particulate matter during a southwest monsoon in Peninsular Malaysia. *Chemosphere* 262:127767. <https://doi.org/10.1016/j.chemosphere.2020.127767>
- Paatero P, Hopke PK (2003) Discarding or downweighting high-noise variables in factor analytic models. *Anal Chim Acta* 490:277–289. [https://doi.org/10.1016/S0003-2670\(02\)01643-4](https://doi.org/10.1016/S0003-2670(02)01643-4)
- Paatero P, Tapper U (1994) Positive matrix factorization: A non-negative factor model with optimal utilization of error estimates of data values. *Environmetrics* 5:111–126. <https://doi.org/10.1002/env.3170050203>
- PAHO (2018) Don't pollute my future! The impact of the environment on children's health. Pan American Health Organization (PAHO) - World Health Organization (WHO). Licence: CC BY-NC-SA 3.0 IGO. Brasília, DF, 2018b. <https://iris.paho.org/handle/10665.2/49123>
- Pant P, Harrison RM (2013) Estimation of the contribution of road traffic emissions to particulate matter concentrations from field measurements: a review. *Atmos Environ* 77:78–97. <https://doi.org/10.1016/j.atmosenv.2013.04.028>
- Peng C, Chen W, Liao X, Wang M, Ouyang Z, Jiao W, Bai Y (2011) Polycyclic aromatic hydrocarbons in urban soils of Beijing: status, sources, distribution and potential risk. *Environ Pollut* 159:802–808. <https://doi.org/10.1016/j.envpol.2010.11.003>
- Pereira GM, Nogueira T, Kamigauti LY, Santos DM, Nascimento EQM, Martins JV, Vicente A, Artaxo P, Alves C, Vasconcellos PC, Andrade MF (2023a) Particulate matter fingerprints in biofuel impacted tunnels in South America's largest metropolitan area. *Sci Total Environ* 159006. <https://doi.org/10.1016/j.scitotenv.2022.159006>
- Pereira GM, Kamigauti LY, Nogueira T, Gavidia-Calderón ME, Monteiro dos Santos D, Evtugina M, Alves C, Vasconcellos PC, Freitas ED, Andrade MF (2023b) Emission factors for a biofuel impacted fleet in South America's largest metropolitan area. *Environ Pollut* 121826. <https://doi.org/10.1016/j.envpol.2023.121826>
- Pereira GM, Oraggio B, Teinilä K, Custódio D, Huang X, Hillamo R, Alves CA, Balasubramanian R, Rojas NY, Sanchez-Ccoylo OR, Vasconcellos PC (2019) A comparative chemical study of PM₁₀ in three Latin American cities: Lima, Medellín, and São Paulo. *Air Qual Atmos Health* 12:1141–1152. <https://doi.org/10.1007/s11869-019-00735-3>
- Pereira GM, Teinilä K, Custódio D, Santos AG, Xian H, Hillamo R, Alves CA, Andrade JB, Rocha GO, Kumar P, Balasubramanian R, Andrade MF, Vasconcellos PC (2017) Particulate pollutants in the Brazilian city of São Paulo: 1-year investigation for the chemical composition and source apportionment. *Atmos Chem Phys* 17:11943–11969. <https://doi.org/10.5194/acp-17-11943-2017>
- Pereira RCC, Pasa VMD (2005) Effect of mono-olefins and diolefins on the stability of automotive gasoline. *Fuel* 85:1860–1865. <https://doi.org/10.1016/j.fuel.2006.01.022>
- Pio C, Cerqueira M, Harrison RM, Nunes T, Mirante F, Alves C, Oliveira C, Sanchez de la Campa A, Artífiano B, Matos M (2011) OC/EC ratio observations in Europe: re-thinking the approach for apportionment between primary and secondary organic carbon. *Atmos Environ* 45:6121–6132. <https://doi.org/10.1016/j.atmosenv.2011.08.045>

- Pio C, Mirante F, Oliveira C, Matos M, Caseiro A, Oliveira C, Querol X, Alves C, Martins N, Cerqueira M, Camões F, Silva H, Plana F (2013) Size-segregated chemical composition of aerosol emissions in an urban road tunnel in Portugal. *Atmos Environ* 71:15–25. <https://doi.org/10.1016/j.atmosenv.2013.01.037>
- Pio CA, Legrand M, Alves CA, Oliveira T, Afonso J, Caseiro A, Puxbaum H, Sanchez-Ochoa A, Gelencsér A (2008) Chemical composition of atmospheric aerosols during the 2003 summer intense forest fire period. *Atmos Environ* 42:7530–7543. <https://doi.org/10.1016/j.atmosenv.2008.05.032>
- Piromal RAS, Rivera-Lombardi RJ, Shimabukuro YE, Formaggio AR, Krug T (2008) Utilização de dados MODIS para a detecção de queimadas na Amazônia. *Acta Amaz* 38:77–83. <https://doi.org/10.1590/S0044-59672008000100009>
- Punshon T, Jackson BP, Meharg AA, Warczack T, Scheckel K, Guerinot ML (2017) Understanding arsenic dynamics in agronomic systems to predict and prevent uptake by crop plants. *Sci Total Environ* 581–582:209–220. <https://doi.org/10.1016/j.scitotenv.2016.12.111>
- Querol X, Alastuey A, Rodriguez S, Plana F, Mantilla E, Ruiz CR (2001) Monitoring of PM₁₀ and PM_{2.5} around primary particulate anthropogenic emission sources. *Atmos Environ* 35:845–858. [https://doi.org/10.1016/S1352-2310\(00\)00387-3](https://doi.org/10.1016/S1352-2310(00)00387-3)
- Ravindra K, Sokhi R, Van Grieken R (2008) Atmospheric polycyclic aromatic hydrocarbons: source attribution, emission factors and regulation. *Atmos. Environ.* 42:2895–2921. <https://doi.org/10.1016/j.atmosenv.2007.12.010>
- Ringuet J, Albinet A, Leoz-Garziandia E, Budzinski H, Villenave E (2012) Reactivity of polycyclic aromatic compounds (PAHs, NPAHs and OPAHs) adsorbed on natural aerosol particles exposed to atmospheric oxidants. *Atmos. Environ.* 61:15–22. <https://doi.org/10.1016/j.atmosenv.2012.07.025>
- Roy R, Braathen NA (2017) The rising cost of ambient air pollution thus far in the 21st century: results from the BRIICS and the OECD countries. OECD Environment Working Papers, No. 124, OECD Publishing, Paris, Publishing, Paris. <https://doi.org/10.1787/d1b2b844-en>
- Saide PE, Gao M, Lu Z, Goldberg DL, Streets DG, Woo J, Beyersdorf A, Corr CA, Thornhill KL, Anderson B, Hair JW, Nehrir AR, Diskin GS, Jimenez JL, Nault BA, Campuzano-jost P, Dibb J (2020) Understanding and improving model representation of aerosol optical properties for a Chinese haze event measured during KORUS-AQ. *Atmos Chem Phys* 20:6455–6478. <https://doi.org/10.5194/acp-20-6455-2020>
- Sanders PG, Xu N, Dalka TM, Maricq MM (2003) Airborne brake wear debris: size distributions, composition, and a comparison of dynamometer and vehicle tests *Environ. Sci Technol* 37:4060–4069. <https://doi.org/10.1021/es034145s>
- Sant’anna A, Alencar A, Pinheiro B, Araújo C, Vormittag E, Wicher H, Borges K, Faria M, Andrade MF, Porto P, Artaxo P, Rocha R, Esturba T, Simoni WF (2021). The state of air quality in Brazil. WRI Brasil. https://www.wribrasil.org.br/sites/default/files/wri-the-state-of-air-quality-in-brazil-executive-_summary_2021.pdf. Accessed 01 June 2021.
- Santanna FB, Almeida-Filho EO, Vourlitis GL, Arruda PHZ, Palácios RS, Nogueira JS (2016) Elemental composition of PM₁₀ and PM_{2.5} for A savanna (cerrado) region of Southern Amazonia. *Quim Nova* 39:1170–1176. <https://doi.org/10.21577/0100-4042.20160154>
- Seinfeld JH, Pandis SN (2006) Atmospheric chemistry and physics: from air pollution to climate change. Wiley, USA
- Serafim E, Besis A, Kouras A, Farias CN, Yera AB, Pereira GM, Samara C, Vasconcellos PC (2023) Oxidative potential of ambient PM_{2.5} from São Paulo, Brazil: variations, associations with chemical components and source apportionment. *Atmos Environ* 298:119593. <https://doi.org/10.1016/j.atmosenv.2023.119593>
- Sharma SK, Mandal TK, Srivastava MK, Chatterjee A, Jain S, Saxena M, Singh BP, Sharma A, Adak A, Ghosh SK (2016) Spatio-temporal variation in chemical characteristics of PM₁₀ over Indo Gangetic plain of India. *Environ Sci Pollut Res* 23:18809–188022. <https://doi.org/10.1007/s11356-016-7025-2>
- Simoneit BRT (1984) Organic matter of the troposphere-III. Characterization and sources of petroleum and pyrogenic residues in aerosols over the western united states. *Atmos Environ* 18:51–67. [https://doi.org/10.1016/0004-6981\(84\)90228-2](https://doi.org/10.1016/0004-6981(84)90228-2)
- Simoneit BRT (2002) Biomass burning — a review of organic tracers for smoke from incomplete combustion. *Appl Geochemistry* 17:129–162. [https://doi.org/10.1016/S0883-2927\(01\)00061-0](https://doi.org/10.1016/S0883-2927(01)00061-0)
- Simoneit BRT, Cardoso JN, Robinson N (1990) An assessment of the origin and composition of higher molecular weight organic matter in aerosols over Amazonia. *Chemosphere* 21:1285–1301. [https://doi.org/10.1016/0045-6535\(90\)90145-J](https://doi.org/10.1016/0045-6535(90)90145-J)
- Singh DK, Kawamura K, Fu P, Kasukabe H, Yanase A, Barrie LA (2021) Photochemical processing of inorganic and organic species in the Canadian high Arctic aerosols: impact of ammonium cation, transition metals, and dicarboxylic acids before and after polar sunrise at alert. *ACS Earth Space Chem* 5:2865–2877. <https://doi.org/10.1021/acsearthspacechem.1c00242>
- Sisenando HA, Medeiros SRB, Saldiva PH, Artaxo P, Hacon SS (2011) Genotoxic potential generated by biomass burning in the Brazilian Legal Amazon by Tradescantia micronucleus bioassay: a toxicity assessment study. *Environ Health* 10:41. <https://doi.org/10.1186/1476-069X-10-41>
- Souza DZ, Vasconcellos PC, Lee H, Aurela M, Saarnio K, Teinilä K, Hillamo R (2014) Composition of PM_{2.5} and PM₁₀ collected at urban sites in Brazil. *Aerosol Air Qual Res* 14:168–176. <https://doi.org/10.4209/aaqr.2013.03.0071>
- Squizzato R, Nogueira T, Martins LD, Martins JA, Astolfo R, Machado C.B., Andrade MF, Freitas ED (2021). Beyond megacities: tracking air pollution from urban areas and biomass burning in Brazil. *npj Clim Atmos Sci* 4:17. <https://doi.org/10.1038/s41612-021-00173-y>
- Tang X, Zhang X, Ci Z, Guo J, Wan J (2016) Speciation of the major inorganic salts in atmospheric aerosols of Beijing, China: measurements and comparison with model. *Atmos Environ* 133:123–134. <https://doi.org/10.1016/j.atmosenv.2016.03.013>
- Thorpe A, Harrison RM (2008) Sources and properties of non-exhaust particulate matter from road traffic: a review. *Sci Total Environ* 400(1–3):270–282. <https://doi.org/10.1016/j.scitotenv.2008.06.007>
- Valente CR, Lacerda-Filho JV, Rizzotto GJ, Bahia RBC, Quadros MLES, Leite SR, Lopes RC, Oliveira IWB, Oliveira CC, Sachs LLB, Silva VA, Batista I (1982) Folha SD.21-Cuiabá, Carta Geológica do Brasil ao Milionésimo, Sistema de Informações Geográficas, Brasil. Geographic Information System, Brazil https://rigeo.cprm.gov.br/bitstream/doc/4987/5/sd21_cuiaba.pdf. Accessed 01 June 2021
- Vasconcellos PC, Artaxo PE, Ciccioli P, Cecinato A, Brancaleoni E, Frattoni M (1998) Determinação dos hidrocarbonetos saturados e policíclicos aromáticos presentes no material particulado da atmosfera Amazônica. *Quim Nova* 21:385–393. <https://doi.org/10.1590/s0100-40421998000400002>
- Vasconcellos PC, Balasubramanian R, Bruns RE, Sanchez-Ccoyllo O, Andrade MF, Flues M (2007) Water-soluble ions and trace metals in airborne particles over urban areas of the state of São Paulo, Brazil: influences of local sources and long-range transport. *Water Air Soil Pollut* 186:63–73. <https://doi.org/10.1007/s11270-007-9465-2>
- Vasconcellos PC, Souza DZ, Ávila SG, Araújo MP, Naoto E, Nascimento KH, Cavalcante FS, Dos Santos M, Smichowski P, Behrentz E (2011) Comparative study of the atmospheric chemical composition of three South American cities. *Atmos*

- Environ 45:5770–5777. <https://doi.org/10.1016/j.atmosenv.2011.07.018>
- Vicente A, Alves C, Calvo AI, Fernandes AP, Nunes T, Monteiro C, Almeida SM, Pio C (2013) Emission factors and detailed chemical composition of smoke particles from the 2010 wildfire season. *Atmos Environ* 71:295–303. <https://doi.org/10.1016/j.atmosenv.2013.01.062>
- Wang G, Zhang R, Gomez ME, Yang L, Levy M, Hu M, Lin Y (2016) Persistent sulfate formation from London Fog to Chinese haze. <https://doi.org/10.1073/pnas.1616540113>
- WHO (2021) WHO global air quality guidelines. 1–360 <https://apps.who.int/iris/bitstream/handle/10665/345334/9789240034433-eng.pdf?sequence=1&isAllowed=y>
- Yamasoe MA, Artaxo P, Miguel AH, Allen AG (2000) Chemical composition of aerosol particles from direct emissions of vegetation fires in the Amazon Basin: Water-soluble species and trace elements. *Atmos Environ* 34:1641–1653. [https://doi.org/10.1016/S1352-2310\(99\)00329-5](https://doi.org/10.1016/S1352-2310(99)00329-5)
- Yang J, Teng Y, Song L, Zuo R (2016) Tracing sources and contamination assessments of heavy metals in road and foliar dusts in a typical mining city, China. *PLoS ONE* 11(12):e0168528. <https://doi.org/10.1371/journal.pone.0168528>
- Yang Q, Chen H, Li B (2015) Polycyclic aromatic hydrocarbons (PAHs) in indoor dusts of Guizhou, southwest of China: status, sources and potential human health risk. *PLoS One* 10:1–17. <https://doi.org/10.1371/journal.pone.0118141>
- Yunker MB, Macdonald RW, Vingarzan R, Mitchell RH, Darcy G, Stephanie S (2002) PAHs in the Fraser River basin: a critical appraisal of PAH ratios as indicators of PAH source and composition. *Org Geochem* 33:1–72. [https://doi.org/10.1016/S0146-6380\(02\)00002-5](https://doi.org/10.1016/S0146-6380(02)00002-5)
- Zhang W, Zhang S, Wan C, Yue D, Ye Y, Wang X (2008) Source diagnostics of polycyclic aromatic hydrocarbons in urban road runoff, dust, rain and canopy throughfall. *Environ Pollut* 153:594–601. <https://doi.org/10.1016/j.envpol.2007.09.004>
- Zhang Y, Zheng H, Zhang L, Zhang Z, Xing X, Qi S (2019) Fine particle-bound polycyclic aromatic hydrocarbons (PAHs) at an urban site of Wuhan, central China: characteristics, potential sources and cancer risks apportionment. *Environ Pollut* 246:319–327. <https://doi.org/10.1016/j.envpol.2018.11.111>
- Zhang ZH, Khlystov A, Norford LK, Tan ZK, Balasubramanian R (2017) Characterization of traffic-related ambient fine particulate matter (PM_{2.5}) in an Asian city: environmental and health implications. *Atmos Environ* 161:132–143. <https://doi.org/10.1016/j.atmosenv.2017.04.040>
- Zhong Q, Zhou Y, Tsang DCW, Liu J, Yang X, Yin M, Wu S, Wang J, Xiao T, Zhang Z (2020) Cadmium isotopes as tracers in environmental studies: a review. *Sci Total Environ* 736:139585. <https://doi.org/10.1016/j.scitotenv.2020.139585>
- Zhou P, Guo J, Zhou X, Zhang W, Liu L, Liu Y, Lin K (2014) PM_{2.5}, PM₁₀ and health risk assessment of heavy metals in a typical printed circuit boards manufacturing workshop. *J Environ Sci (China)* 26:2018–2026. <https://doi.org/10.1016/j.jes.2014.08.003>

Publisher's note Springer Nature remains neutral with regard to jurisdictional claims in published maps and institutional affiliations.

Springer Nature or its licensor (e.g. a society or other partner) holds exclusive rights to this article under a publishing agreement with the author(s) or other rightsholder(s); author self-archiving of the accepted manuscript version of this article is solely governed by the terms of such publishing agreement and applicable law.